### Title

Chapter 12 Mixing in the Southern Ocean




### Authors

Gille, Sarah T
Sheen, Katy L
Swart, Sebastiaan
et al.



### Publication Date

2022

### DOI

10.1016/b978-0-12-821512-8.00019-0

Peer reviewed

Chapter 12

# Mixing in the Southern Ocean

**Sarah T. Gille[a], Katy Sheen[b], Sebastiaan Swart[c,d], and Andrew F. Thompson[e]**

*[a]Scripps Institution of Oceanography, University of California San Diego, USA, [b]Penryn Campus, University of Exeter, England, [c]Department of Marine Sciences, University of Gothenburg,Gothenburg, Sweden, [d]Department of Oceanography, University of Cape Town, Rondebosch, South Africa, [e]Environmental Science and Engineering, California Institute of Technology, Pasadena, USA*

**ABSTRACT**

Southern Ocean mixing helps to establish properties of the global ocean both by blending waters from the northern basins and through local water mass formation. Air-sea fluxes of heat, momentum, freshwater, and gas are responsible for mixing and transformation of water properties at the ocean surface. Transient storms and submesoscale motions influence the timing and magnitude of upper ocean mixing and exchange with the interior. In the Southern Ocean, along-isopycnal stirring by eddies connects the ocean surface with the mid-depth to deep interior. Interior mixing is largely adiabatic but spatially heterogeneous in both vertical and horizontal directions with eddy diffusivities estimated to vary by a factor of four or more, from roughly 700 to 2800 $m^2\ s^{-1}$. Regions of strong stirring and strain are concentrated above and downstream of major bathymetric features. Small-scale turbulent mixing in the ocean interior is driven by internal waves, generated through flow–topography interactions, and turbulent mixing is enhanced in the bottom boundary layer. The marginal ice zones around Antarctica and processes on the Antarctic shelf are mixing regimes unique to the Southern Ocean that remain frontiers of current research.

**KEYWORDS**

Southern Ocean, Air-sea fluxes, Water mass transformation, Sea ice, Submesoscale, Diapycnal mixing, Isopycnal mixing, Marginal ice zone, Lee waves, Bottom-intensified dissipation

## 12.1 INTRODUCTION

The Southern Ocean connects the components of the global ocean, and this makes it central to global ocean mixing. The eastward-flowing Antarctic Circumpolar Current (ACC) provides a horizontal link between the Atlantic, Indian, and Pacific Oceans. The Southern Ocean also connects low and high southern latitudes along the steeply tilted isopycnal surfaces of the ACC. Since water parcels preferentially mix along isopycnals (see Chapter 9), the Southern Ocean

provides a key route between the ocean surface and the deep interior. In addition, the Southern Ocean connects ocean waters with the ice shelves that surround the Antarctic continent. Mixing processes on the Antarctic continental shelf help to determine the rate at which these ice shelves melt and how much freshwater enters the ocean. Any turbulent mixing that changes water mass properties—whether resulting from buoyancy forcing at the ocean surface, processes associated with tides and bathymetry deep below the ocean surface, or interactions with the cryosphere—has the potential to have a disproportionate impact on global ocean properties and therefore large-scale climate and ecosystems.

This chapter builds on earlier chapters to examine how a range of mixing processes shape the Southern Ocean circulation and climate. Our focus here is centered on the impact of physical processes on mixing rates. An overview of how Southern Ocean mixing influences the climate system is found in Chapter 2, and a review of the Southern Ocean's role in the large-scale ocean circulation is found in Chapter 3. Some of the mixing processes that are critical to Southern Ocean dynamics receive individual treatment in other chapters, and we have provided references to those in the text that follows. Here, section 12.2 reviews the large-scale context framing Southern Ocean mixing. We then move through the water column, starting with turbulent mixing near the ocean surface in section 12.3, regional and mesoscale interior mixing in section 12.4, and small-scale turbulence in the ocean interior in section 12.5. Each section presents the foundations underlying the science and then highlights recent findings. A sidebar highlights how the Diapycnal and Isopycnal Mixing Experiment in the Southern Ocean (DIMES) brought together multiple observing capabilities and modeling strategies to advance understanding of Southern Ocean mixing. The chapter concludes with perspectives on emerging science challenges for the future.

## 12.2 LARGE-SCALE CONTEXT: FOUNDATIONS

Large-scale circulation in the Southern Ocean is distinct from large-scale circulation in other parts of the global ocean because of the gap in continental boundaries in the latitude range of Drake Passage (56°–63°S). Eastward winds provide a continuous band of surface momentum forcing all the way around Antarctica. Because of the Coriolis effect, an eastward wind stress at the Southern Ocean surface results in northward Ekman transport of surface waters, carrying cold high-latitude surface water toward the subtropics (e.g. Toggweiler and Samuels, 1998). This Ekman advection establishes a north–south gradient in sea surface height, with elevated sea surface height to the north. The corresponding top-to-bottom meridional pressure gradient supports an eastward geostrophic flow, known as the Antarctic Circumpolar Current (ACC, black arrow in Fig. 12.1). The absence of topographic barriers above roughly 2000 m and the limited ability to sustain large-scale zonal pressure gradients above these depths allow the ACC to maintain mean meridional density gradients: density surfaces that are deep at the northern boundary of the ACC shoal to the south.

The surface water carried northward as Ekman transport is replaced with water that upwells within the ACC. (The upwelling is attributed to Ekman pumping due to wind-stress divergence.) This upwelled Circumpolar Deep Water (CDW) is transported and mixed through eddy motions along the Southern Ocean's steeply tilted isopycnals (light blue CDW in Fig. 12.1) from mid-depth (around 2000-3000 m depth) in the subtropics to the surface within the Southern Ocean. Along-isopycnal pathways thus provide a direct connection between the surface and the mid-depth ocean interior. (See Chapter 9 for a more detailed exploration of isopycnal mixing.) The Southern Ocean is host to approximately 70% to 80% of upwelling of global deep waters to the sea surface (DeVries and Primeau, 2011; Talley, 2013). Along-isopycnal mixing plays a central role in the climate system: modeling studies have for many years highlighted the sensitivity of Southern Ocean circulation to the representation of this mixing (e.g. Redi, 1982; Danabasoglu et al., 1994; Danabasoglu and McWilliams, 1995; Griffies, 1998; Gent, 2016). Together interior upwelling and northward surface advection constitute the upper cell of the Southern Ocean's meridional overturning circulation (MOC) (Speer et al., 2000).

The lower cell of the Southern Ocean meridional overturning comprises denser CDW, known as Lower Circumpolar Deep Water (LCDW) that upwells across the ACC but outcrops at the surface on the southern side of the ACC (Marshall and Speer, 2012). Water that upwells here loses heat to the atmosphere, while also increasing its salinity as a result of brine rejection during sea ice formation to form Antarctic Bottom Water (AABW) that sinks to the sea floor (dark blue arrow in Fig. 12.1), providing a direct connection between the atmosphere and the deep ocean. Mixing processes in the lower cell occur in the subpolar gyres (e.g. Vernet et al., 2019), over the Antarctic continental slope (e.g. Stewart and Thompson, 2013; Heywood et al., 2014), and over the continental shelf, where they are modulated by tides (e.g. Padman et al., 2018; Stewart et al., 2018) as well as by complex topography and by interactions between sea ice, ice shelves, and the ocean (e.g. Gille et al., 2016).

The connection between the deep ocean and the surface is further supported by the Southern Ocean's low stratification: as temperatures drop, ocean density is progressively less dependent on temperature, and at temperatures colder than about 2°C, salinity is the dominant controller of oceanic potential density (e.g. Nycander et al., 2015), such that surface-to-bottom temperature differences result in little difference in potential density. Cold temperatures of the Southern Ocean offer ideal conditions for low vertical stratification, particularly in regions such as the ACC latitudes, where freshwater inputs from precipitation or melting ice are minimal. As a result the Southern Ocean is generally weakly stratified and forms deep mixed layers (Dong et al., 2008; Holte et al., 2017; Speer et al., 2018) that allow small energy inputs to readily mix the ocean vertically.

The region also experiences significant horizontal stirring. The ACC consists of multiple narrow jets that roughly follow zonal pathways located between about 40° and 60°S. From north to south, the jets coincide with individual density

gradients that are referred to as the Subantarctic Front, the Polar Front, and the Southern ACC Front (Orsi et al., 1995). These frontal jets extend from the surface to the sea floor and are steered by topography. They can meander substantially, and at times they may split or merge so that there are more or less than three jets in some locations (Sokolov and Rintoul, 2009; Thompson and Sallée, 2012). The ACC jets are energetic enough to be baroclinically unstable, and interactions with topography are associated with flow instabilities that spawn transient eddies and heightened levels of eddy kinetic energy (EKE) (e.g. Meredith and Hogg, 2006; Hogg et al., 2008), influencing the Southern Ocean heat budget. In most of the global ocean, western boundary currents are responsible for the poleward transport of energy that is input by the sun in the tropics. However, in the Southern Ocean mean southward transport of heat is impeded by the absence of continental boundaries at the latitude of Drake Passage (55°-6-°S), and instead eddies play a leading role in the poleward transport of heat south of 40°–50°S (e.g. deSzoeke and Levine, 1981; Keffer and Holloway, 1988; Johnson and Bryden, 1989; Ivchenko et al., 1996; Gille, 2003; Meijers et al., 2007; Volkov et al., 2010).

The ease with which the Southern Ocean mixes gives it a central role in the climate system. Recent observations indicate that the Southern Ocean is gaining heat more rapidly than other regions of the global ocean (e.g. Roemmich et al., 2015), although sea surface temperatures show evidence of cooling (Armour et al., 2016). The Southern Ocean has also been implicated as the major location for oceanic uptake of $CO_2$ (e.g. Caldeira and Duffy, 2000; Sabine et al., 2004; Gruber et al., 2019). Attribution studies suggest that the observed warming is due to heat uptake from the atmosphere within the Southern Ocean rather than advection within the ocean (Swart et al., 2018a). This implies that upper-ocean turbulence mediates much of the long-term oceanic change, but that horizontal advection also matters. Climate simulations suggest that correctly representing the uptake of heat and carbon in the Southern Ocean is critical: multi-model assessments indicate that climate at the end of the century depends on the present structure of the ocean mixed layer and thus the mixing within the upper ocean (e.g. Boé et al., 2009), and that ocean heat uptake is sensitive to the representation of air-sea fluxes (e.g. Huber and Zanna, 2017). Mixing processes not only close the global overturning circulation but are also fundamentally important for oceanic exchange of carbon and heat (e.g. Watson and Naveira Garabato, 2006; Morrison et al., 2016), nutrient resupply for sustaining oceanic biological production (e.g. Pollard et al., 2006), and the melt rate of ice shelves (e.g. Silvano et al., 2018).

The Southern Ocean is unique in the ways that different mixing processes impact the region's circulation. For instance, nowhere else is such a broad range of density classes ventilated at the ocean surface. This supports a significant fraction of the water mass transformation associated with the global overturning circulation. The ACC also hosts strong deep-ocean currents (Chereskin et al., 2009; Fukamachi et al., 2010) and, through their interaction with large bathy-

metric features, generates distinct mixing processes. Finally, along-isopycnal mixing is the dominant process that delivers waters toward and away from key sites of water mass transformation at the ocean surface, over sloping topography, and on the continental shelf. In the remainder of this chapter, we offer an overview of these different components of Southern Ocean mixing and identify priorities for future research.

## 12.3 UPPER CELL: MIXED-LAYER TRANSFORMATIONS

### 12.3.1 Foundations and setting

Surface mixing in the Southern Ocean is of particular importance to the climate system because the cold, dense water that outcrops here has nearly the same potential density as deeper waters throughout the global ocean. The ventilation of these dense, near-surface waters means that surface mechanical and buoyancy forcing has the potential to set interior water properties.

Upper-ocean mixing processes maintain the surface mixed layer as the buffer layer through which all exchanges of mass and energy pass between the ocean and atmosphere. The surface mixed layer is analogous to a 'vestibule' between the atmosphere and the ocean. Air-sea fluxes bring properties (e.g. heat, freshwater, and $CO_2$) into the mixed layer. Mechanisms at work in the mixed layer, such as adiabatic advection, stirring, turbulent diffusion and convection, ultimately determine whether these properties are re-emitted to the atmosphere or enter the ocean interior—figuratively whether properties pass through the vestibule into the ocean interior.

Characteristics of the Southern Ocean that are conducive to energetic upper-ocean mixing include first, the presence of lateral gradients in temperature, salinity, or density, associated with hydrographic fronts and mesoscale eddies, and second, the weak stratification of the region that allows deep mixed layers to form seasonally (Dong et al., 2008; Holte et al., 2017) supporting vertical mixing between the upper ocean and the thermocline.

Overlying this energetic ocean environment is an atmosphere characterized by strong and variable winds and heat fluxes that promote atmosphere–ocean interactions. The surface experiences a strong time-mean wind stress (momentum flux) associated with a band of maximum wind forcing (Lin et al., 2018) induced by transient Southern Ocean storms, with near-surface wind speeds often exceeding 20 m $s^{-1}$ (Yuan, 2004). Storms add a time-varying and rotational component to the background wind forcing, which can interact directly with the lateral density gradients and induce Ekman pumping and shear-driven mixing. In addition, seasonal air-sea and air-sea-ice fluxes of heat and freshwater change the buoyancy budget of the mixed layer, which as we will see later in this chapter, can enhance or arrest mixing processes within and below the thermocline and are thus important for the ventilation of the lower thermocline. Figure 12.2 encapsulates a broad range of processes that influence surface boundary layer

properties and their exchange with the interior.

### 12.3.2 Mixing in the surface boundary layer and connection to subsurface adiabatic stirring

#### *12.3.2.1 Surface water mass transformation:*

A significant proportion of upper-ocean mixing and mixed-layer properties can be ascribed to relatively simple one-dimensional physical responses to surface momentum and buoyancy fluxes (Price et al., 1978; Large et al., 1994). Studies of surface boundary layer turbulence have historically been weighted to Northern Hemisphere conditions. (For fundamentals, see Chapter 4 for discussion of surface layers and Chapter 5 for surface-generated internal waves.) More recent observations are allowing us to understand mixed-layer budgets in various regions of the Southern Ocean, including sea-ice impacted regions, albeit at relatively coarse resolution (Pellichero et al., 2017). Surface forcing mechanisms are exceptionally strong in the Southern Ocean and are characterized by distinct seasonal cycles of sea-ice freshwater and air-sea heat fluxes that are the primary drivers for surface salinity and temperature variations (Pellichero et al., 2017).

During austral winter, high levels of heat loss by the ocean can lead to deep convective mixing, resulting in deep mixed layers (Holte et al., 2012). This is particularly the case at the northern edge of the ACC (north of Subantarctic Front) where mixed layers can exceed depths of 700 m in winter (Dong et al., 2008; Tamsitt et al., 2020). Heat loss events are intermittent, and most of the annual mixed-layer deepening appears to occur during a small number of events (Ogle et al., 2018). These strong air-sea exchanges lead to water mass transformation at the surface and are a leading order driver of Sub-Antarctic Mode Water (SAMW) formation and its interannual variability (Naveira Garabato et al., 2009). In addition, the formation rate and characteristics of SAMW are also influenced by diapycnal mixing (Sloyan et al., 2010), eddy-induced transport and upwelling (Marshall, 1997; Sallée et al., 2010), and the large-scale Ekman transport of cool, low salinity water equatorward across the Subantarctic Front (Rintoul and England, 2002).

#### *12.3.2.2 Submesoscale-induced mixing and stratification:*

Upper-ocean stratification and mixing rates are also impacted by complex, horizontal processes in response to fronts, eddies and jets. These horizontal dynamics occur at small spatial scales that extend down to the submesoscale (0.1–10 km, hours–days; Figure 12.2; see Chapter 8 for a more comprehensive description of submesoscale processes). Submesoscale mixing is enhanced by the factors that characterize the Southern Ocean's mixing-favorable conditions: strong surface forcing, persistent lateral buoyancy gradients, weak vertical stratification, and deep mixed layers.

Initial understanding of the role of submesocales in the Southern Ocean re-

lied on submesoscale-resolving simulations for specific regions including Drake Passage (Bachman et al., 2017) and Kerguelen Plateau (Rosso et al., 2014). These numerical studies showed that submesoscales directly impact upper-ocean stratification, for example through mixed-layer shoaling with increased model resolution (Bachman et al., 2017) and through vertical exchanges between the surface layer and ocean interior (Rosso et al., 2014, 2015; Balwada et al., 2018; Su et al., 2018; Bachman and Klocker, 2020).

Observations have further highlighted the role of submesoscale instabilities. Using ship-based measurements along the edges of a large mesoscale eddy pinched off from the Polar Front, Adams et al. (2017) identified the presence of submesoscale instabilities that can lead to strong net subduction of water associated with fine-scale dense outcropping filaments. Submesoscale Rossby waves, found along the ACC, also drive intense vertical circulations (Taylor et al., 2018). These recent observations emphasize the importance of larger scale adiabatic stirring at mesoscales (McWilliams, 2016) that catalyze submesoscale mixed-layer instabilities in the Southern Ocean, thereby providing a connection between the surface boundary layer and the ocean interior (Erickson et al., 2020), as biogeochemical tracers have demonstrated in the open ocean (Llort et al., 2018). Months-long glider-based surveys in the Southern Ocean have been used to estimate the presence and strength of submesoscale flows in the upper ocean. Mixed-layer eddies (MLE; Figure 12.2) are expected to proliferate where mixed layers are deep in the Southern Ocean, particularly in the presence of sharp lateral buoyancy gradients. Slumping MLEs can rearrange horizontal buoyancy gradients to vertical stratification through an ageostrophic secondary circulation (see Chapter 8; Fox-Kemper et al., 2008). Observations show that MLEs can arrest mixing in the Southern Ocean and induce springtime mixed-layer stratification earlier than would be possible with surface buoyancy forcing alone (du Plessis et al., 2017). The impact of the submesoscale on upper-ocean stratification is also spatially heterogeneous due to its dependence on the background mesoscale eddy field. For instance, Viglione et al. (2018) found an abrupt transition in the strength of the submesocale eddy field, delineated by the Shackleton Fracture Zone. Despite this topographic feature having a sill depth thousands of meters below the surface, it gives rise to different mesoscale stirring regimes that impact surface boundary layer dynamics, including the potential for more vigorous mixing processes, such as symmetric instability, occurring downstream of the Fracture Zone, but not upstream.

Submesoscale processes cannot be easily disentangled from the Southern Ocean's intense storm systems and associated wind stress at the surface (e.g. Klocker, 2018). Under the action of wind, submesoscale flows are influenced by fine-scale cross-frontal horizontal Ekman advection of water of different density (Ekman Buoyancy Flux, EBF; Figure 12.2; Chapter 8). In the case of down-front wind conditions, cross-frontal Ekman flows that carry denser waters over the lighter side of the front can force convective instabilities and enhance mixing through small-scale turbulence. This can increase dissipation within

and across the mixed layer by an order of magnitude compared to wind-driven shear mixing (Thomas, 2005). When the opposite occurs during up-front winds, light water is advected over the dense water on the other side of the front, mixing can be arrested, and the mixed layer can shoal. The Southern Ocean's prevailing westerly winds, oriented along the mean frontal flows associated with the ACC, make these wind-front processes particularly relevant (Johnson et al., 2016), with average down-front wind conditions occurring in the Southern Ocean and providing a significant destratifying and mixing flux to the surface ocean (du Plessis et al., 2019; Viglione et al., 2018; Giddy et al., 2021). This effect of EBF is large enough to delay the onset of springtime stratification by two months after the onset of seasonal surface heating and to eradicate half the stratification gained by surface buoyancy forcing (du Plessis et al., 2019). The major topographic features in the Southern Ocean regionally deflect the average frontal flow away from the prevailing wind direction, allowing for strong variability in mixing and rates of stratification across the open-ocean extent of the Southern Ocean. This heterogeneous characteristic of submesoscale processes and its impact on the timing of seasonal restratification is likely to have significant impacts on spring phytoplankton blooms and timing (Carranza and Gille, 2015; Swart et al., 2015; Pellichero et al., 2020).

Storms are known to induce energetic, "instantaneous," vertical mixing events in the Southern Ocean, with upper-ocean vertical eddy diffusivity, $K_z \sim O(10^{-1}\ \mathrm{m^2\ s^{-1}})$ (Cisewski et al., 2005; Forryan et al., 2015). This mixing contributes to energizing and deepening the surface mixing layer. Wind-driven energy has also been shown to excite strong inertial motions within the upper ocean, which may last several days to weeks post storm and result in enhanced shear-driven vertical mixing below the base of the mixing layer within a "mixing transition" layer (Forryan et al., 2015). In the presence of mesoscale and submesoscale variability, this wind-driven inertial energy is concentrated (e.g. Klein et al., 2004; Jing et al., 2011; Meyer et al., 2015) and may further impact the extent and magnitude of the transitional mixing layer (Alford et al., 2016). Ultimately these small-scale features and their interactions with surface wind stress (storm-eddy interactions, Figure 12.2) enhance the downward propagation of inertial energy into the subsurface ocean (Jing et al., 2011) and potentially induce the rapid breaking of near-inertial waves to produce intense vertical mixing in the Southern Ocean (Meyer et al., 2015) that can extend below the base of the mixed layer (Forryan et al., 2015). Further studies using both 1D and 3D model simulations have explored the interaction of mixing with mesoscale-to-submesoscale eddy stirring (Uchida et al., 2019, 2020) and the impact of the interior mixing due to inertial motion set by passing storms in the Southern Ocean (Jouanno et al., 2016; Nicholson et al., 2016, 2019; Whitt et al., 2019). These findings suggest that inertially driven subsurface mixing may persist for several days to weeks after a passing storm, and after the deepened active mixing layer has restabilized to the surface. Such intraseasonal mixing processes are proving important to biogeochemical cycles, with summer primary productivity

in the Southern Ocean considerably enhanced and sustained, largely due to the supply of deep iron reservoirs below the mixed layer (Carranza and Gille, 2015; Swart et al., 2015; Whitt et al., 2017; Nicholson et al., 2019; Uchida et al., 2020).

Although these mechanisms are theorized and modelled to be important in the Southern Ocean, direct observations (Chapter 14) of these interactions are sparse. It thus remains uncertain how storm-driven mixing energy will alter the magnitude and shape of the mean upper-ocean vertical diffusion profiles particularly in a dynamically complex ocean. Measurements of subsurface mixing are limited to microstructure data collected during summer periods (e.g. Forryan et al., 2015), emphasizing the need to constrain these mixing rates in other seasons, especially in winter when mixing rates are expected to increase significantly.

#### *12.3.2.3 Interactions between sea ice and Southern Ocean mixing*

Sea ice covers a vast portion of the Southern Ocean with a winter maximum extent exceeding 18 million $km^2$, and it is an important influence on surface boundary layer processes. Observations of upper-ocean mixing and variability remain sparse in this region, contributing to both a poor mechanistic understanding of coupled ocean-ice-atmosphere processes and large uncertainty in model representations of sea ice impact on larger-scale climate. Under sea ice or within regions of recent sea ice melt, the surface sea ice cap or surface freshwater lens are expected to suppress mixing and submesoscale energetics. However, sea ice melt and associated freshwater fluxes (Abernathey et al., 2016; Haumann et al., 2016; Pellichero et al., 2018) can also strengthen lateral buoyancy gradients, stimulating submesoscale flows.

High-resolution observations using autonomous platforms at the edge of the Antarctic sea ice have revealed sub-kilometer sized submesoscale fronts, hypothesized to be driven by the stirring of the fresher surface layer by mesoscale eddies, which remain active throughout the spring-summer melt season (Swart et al., 2020; Giddy et al., 2021). These upper-ocean flows are shown to be intricately coupled to surface winds: strong winds (storms) increase shear stresses, which drive mixing and reduce lateral buoyancy gradients (Swart et al., 2020). Scientific tags attached to elephant seals have been used to identify the presence of submesoscale flows under sea ice in the middle of winter: Biddle and Swart (2020) postulated that during sea ice formation, brine-rejection-induced convective mixing can erode the halocline and introduce lateral buoyancy gradients that catalyze submesoscale motions. Similarly, the presence of leads (gaps between sea ice floes; e.g. Fons and Kurtz, 2019) allows for lateral heterogeneity in ocean-atmosphere interaction that adjusts the surface buoyancy and stresses, promoting both convective and submesoscale-induced mixing (Figure 12.2). Whether these processes are intermittent or quasi-permanent, they are likely to generate vertical fluxes of heat and salt (Thomas et al., 2008) that will alter the buoyancy and heat budget of the upper ocean, further adjusting sea ice melt and

formation rates. This is especially relevant in the Antarctic marginal ice zone and especially at the Antarctic Shelf break, where warm and salty Circumpolar Deep Water (CDW) lies closely under the surface mixed layer, increasing the potential for water mass transformation. Furthermore, recent observations in the Ross Gyre reveal the presence of double-diffusive staircase structures underlying the surface mixed layer and the potential for these processes to regulate sea ice thickness (Bebieva and Speer, 2019), suggesting the feedback between sea ice and mixing in these systems. (See Chapter 11 for further discussion on double diffusion in ice-covered regimes.)

Flow-topography interactions occurring under sea ice can enhance upward heat transport and generate eddies that exert divergent strain on the sea ice cover (see Kurtakoti et al., 2018) causing the sea ice thickness to decrease and on sporadic occasions initiating open-water polynyas (Figure 12.2), such as those documented in the Weddell Sea (Gordon, 1978; Holland, 2001). This, together with intense winter storm conditions and a frigid overlying atmosphere, results in a loss of surface buoyancy, generating vigorous convective mixing and overturning (Wilson et al., 2019), with heat and saline waters (CDW) lying just below the cold surface layer (Gordon, 1978). Most recently, the Maud Rise polynya in 2016 and 2017 was fortuitously sampled by Argo floats deployed as part of the Southern Ocean Carbon and Climate Observations and Modeling (SOCCOM) project. These observations showed periods of absent vertical stratification (near-zero buoyancy frequency) reflecting recent mixing with the winter surface waters, as well as intermediate layer water mass intrusions resembling submesoscale coherent vortices at significant depth (Campbell et al., 2019; Swart et al., 2018b). In addition, the effect of thermobaricity (Akitomo, 1999) may have modulated the depth of mixing by supplying additional kinetic energy to plumes descending across the pycnocline. In combination, the processes occurring in polynyas short-circuit conventional pathways to water mass transformation and ventilation by connecting the surface boundary layer with the abyssal ocean through exceptionally high rates of deep (4000 m) winter convection (Martinson and Iannuzzi, 1998).

## 12.4 INTERIOR MIXING: REGIONAL AND MESOSCALE PROCESSES

### 12.4.1 Foundations: Southern Ocean eddy pathways

The characteristics of lateral mixing in the Southern Ocean are apparent from any snapshot of two key physical properties: variability in the ocean's sea surface height (SSH) distribution and the tilt of Southern Ocean isopycnals as they plunge from the base of the surface boundary layer into the ocean interior at the ACC's northern boundary. These two properties are intricately linked and a signature of the importance of the eddy variability that dominates interior mixing in the Southern Ocean. At all longitudes, SSH increases broadly from south to north across the ACC with a slope of a couple millimeters per kilometer —

sufficient to support the strongest current in the global circulation system. Yet this SSH slope, which provides information on the surface circulation through geostrophic balance, is far from uniform across the ACC. In certain locations, SSH undergoes a few abrupt jumps from south to north, separated by flat regions hundreds of kilometers wide. In other regions, the meridional profile of SSH is evocative of a washboard, rising northward in a series of bumps and wiggles. Measurements made from satellite altimeters have been the primary tool for studying mesoscale mixing in the Southern Ocean (e.g. Hughes and Ash, 2001), revealing how contours of SSH meander and pinch off in coherent vortices, periodically compress together and fan out to accommodate the complex bathymetry below.

The spatial distribution of SSH is mirrored in an inverse sense by the south-to-north deepening of density surfaces in the ACC. Although isopycnal surfaces are more difficult to observe than SSH, hydrographic transects show that they often appear as a staircase with regions of risers and steps providing a signature of the sinuous jets that comprise the ACC system. This complex topology of the Southern Ocean SSH and density field provides insight into the various mechanisms by which properties are stirred and advected laterally and vertically across the Southern Ocean and will be the primary focus of this section.

Throughout the ocean, mesoscale dynamics are critical for the adiabatic, or along-isopycnal, stirring of tracers (see Chapter 9). While in most regions adiabatic stirring is synonymous with lateral transport, mesoscale processes take on an added importance in the Southern Ocean. The isopycnal tilt across the ACC provides a large source of available potential energy (APE) that sustains the relatively high levels of eddy kinetic energy (EKE) in the Southern Ocean. This density structure and the associated baroclinic transport of the ACC appears remarkably insensitive to climate forcing due to the interplay between the mechanical source of APE from the wind stress and baroclinic instability that persistently converts APE to kinetic energy in the form of mesoscale eddies (Hallberg and Gnanadesikan, 2006; Marshall et al., 2017). Critically for the climate system, the sustained tilting of isopycnals provides a pathway for adiabatic advection and stirring to transport tracers vertically through the water column and thus ventilate the deep ocean interior in the absence of diabatic mixing of surface and subsurface waters (see also the more extended discussions in Chapters 2 and 3).

There are two mechanisms by which spatially and temporally varying eddies may transport a tracer $C$ across the ACC within a density class with a thickness $h$. A meridional isopycnal flux can be decomposed as follows:

$$\frac{\overline{vhC}}{\overline{h}} = \overline{v'h'}\frac{\overline{C}}{\overline{h}} + \overline{v'C'} + \frac{\overline{v'h'C'}}{\overline{h}}, \tag{12.1}$$

where $v$ is the meridional velocity, overbars indicate a zonal and/or temporal average over scales larger than the characteristic eddy scale, primes indicate a deviation from the average, and we have assumed that $\overline{v} = 0$. The triple cor-

relation term on the right-hand side of (12.1) is typically assumed to be small. The first term on the right-hand side arises from the correlation of velocity fluctuations and buoyancy anomalies, or equivalently thickness anomalies, that gives rise to a mass or volume transport (Marshall and Radko, 2003; Marshall and Speer, 2012). When combined with the background tracer distribution, this gives rise to an eddy advective flux, typically represented in coarse resolution numerical simulations by the Gent and McWilliams (1990) parameterization. Note that this eddy thickness flux supports both upwelling and downwelling branches of the overturning circulation, which in steady state, is determined by the combined distribution of the surface buoyancy and the surface buoyancy flux fields (Marshall, 1997; Marshall and Radko, 2003; Abernathey et al., 2016). The second term on the right of (12.1) indicates that even when the overturning circulation is weak (*e.g.* wind and eddy overturning circulations balance), eddy stirring along density surfaces will homogenize tracer distributions via down-gradient tracer fluxes (Abernathey and Ferreira, 2015), most commonly parameterized as an eddy diffusivity (Redi, 1982).

An important and active research question asks whether these density layers act as adiabatic pathways or whether they are "leaky." Diabatic mixing is discussed in section 12.5, and is a key component of the Southern Ocean circulation, especially where strong frontal circulations interact with topographic features. Nevertheless, mixing processes in the upper part of the ACC are typically assumed to be largely adiabatic, although some studies have questioned this assumption (Sun et al., 2018). The case for weak modification in the upper ACC is provided by Nikurashin and Vallis (2011) who argued from a scaling analysis that the residence time of a fluid parcel as it traverses the ACC is short compared to the time scales associated with vertical displacement due to diapycnal mixing. In the following subsection, we explore the processes that enable tracers to spread along density surfaces. While the discussion above emphasizes a two-dimensional (depth-latitude) framework, the combination of a heterogeneous distribution of EKE with a strong zonal mean flow implies that mixing is an intermittent process as water parcels trace out complicated three-dimensional trajectories spiraling both toward and away from Antarctica (Tamsitt et al., 2017).

### 12.4.2 Mixing and coherent structures: Adiabatic recipes for Southern Ocean mixing

Progress on the dynamical properties of the ACC has taken advantage of its circumpolar nature, decomposing the flow into zonal averages and departures from this mean, as in (12.1) above. Strikingly, the distribution of EKE throughout the entire Southern Ocean is patchy and strongly influenced by the interaction of frontal currents with topographic features. Through the use of satellite altimetry data, key features of the EKE distribution have been studied (e.g. Gille and Kelly, 1996). The bathymetry of the Southern Ocean varies across a range of scales, but there are a discrete number of topographic features that enforce a significant

deviation in the ACC's zonal flow. These include the Scotia Arc, the Southwest Indian Ridge, Kerguelen Plateau, Macquarie Ridge and Campbell Plateau, and the Pacific-Antarctic Ridge. At each of these locations, EKE is elevated in the lee of the topographic feature and suppressed in front of the feature (Witter and Chelton, 1998). The region of enhanced EKE typically extends 500 to 1000 km downstream of the topography, encompassing a region that is nearly an order of magnitude larger than a typical coherent mesoscale eddy (Lu and Speer, 2010). The mean flow in these elevated EKE regions is often associated with meridional displacements of the ACC streamlines (contours of SSH) that are largely steady, leading to their distinction as standing meanders that have been compared to atmospheric storm tracks (Abernathey and Cessi, 2014; Bischoff and Thompson, 2014; Chapman et al., 2015).

Explanations for the elevated EKE within standing meanders have focused on the role of baroclinic instability. Steering of the mean flow by bathymetry generates a standing meander that locally increases lateral buoyancy gradients in the vicinity of the ridge and provides an enhanced source of APE that feeds eddy growth (Fig. 12.3a; Abernathey and Cessi, 2014). Additionally, standing meanders can sustain a mean-flow configuration with a substantial meridional component (Fig. 12.4). These non-zonal flows are susceptible to linear instabilities that grow faster than unstable modes of purely zonal flows (Smith, 2007). The distribution of EKE is also shaped by the propagation of the growing instability as it is advected downstream by the mean flow (Pierrehumbert, 1984; Bracco and Pedlosky, 2003). Enhancement of the lateral buoyancy gradients in and around standing meanders is a consequence of conservation of potential vorticity that squeezes the mean flow as it flows northward and over shallower bathymetry (Patmore et al., 2019). This structure not only increases the baroclinicity of the flow, but also results in strong horizontal velocity shear on the flanks of the frontal current that can lead to barotropically unstable flow configurations. Both Youngs et al. (2017) and Barthel et al. (2017) have argued that close to topographic features, barotropic or mixed barotropic-baroclinic instabilities can dominate over baroclinic instability. The distinction between EKE generated from these two different instabilities has implications for both the energy budget and the large-scale stratification of the ACC. For instance, the release of potential energy via baroclinic instability gives rise to eddy buoyancy fluxes that support the vertical transfer of momentum from the ocean surface to the seafloor via interfacial form stress (Treguier and McWilliams, 1990; Olbers et al., 2004) (Fig 12.4), whereas barotropic instabilities are mediated by eddy momentum fluxes (Youngs et al., 2017). The localization of eddy fluxes also impacts the closure of the Southern Ocean meridional overturning circulation. The large-scale balance between wind- and eddy-overturning cells that comprises the zonally averaged residual arises from localized regions where eddies dominate and isopycnal tilt is relaxed, followed by regions where Ekman overturning dominates and isopycnals steepen again (Thompson and Naveira Garabato, 2014). Finally, Mazloff et al. (2013) argued that a third component, separate from the

wind/eddy cells, arises from the outcropping of isopycnals at the sea surface and bathymetric features. This outcropping allows for the development of time-mean pressure gradients and a mean geostrophic gradients, which in the presence of strong boundary diabatic processes, can make a substantial contribution to the total overturning. Mazloff et al. (2013) suggested that this mean component is indeed dominant following a large cancellation of the other terms; it would be of interest to re-visit this analysis using a fully eddy-resolving simulation.

The shaping of the EKE distribution by flow–topography interactions highlights the finding that lateral transport across the ACC is an intermittent process. An understanding of spatial variations in Southern Ocean mixing properties arose, in part, to reconcile observed patchy EKE distributions with traditional methods of defining Southern Ocean fronts as circumpolar features (Orsi et al., 1995; Sokolov and Rintoul, 2009). Marshall et al. (2006) used altimetry-derived surface velocities to advect a passive tracer and arrived at a near-surface eddy diffusivity estimate using an "effective diffusivity" approach that quantifies tracer-contour complexity. This study found an eddy diffusivity that varied between 500 and 2000 $m^2\ s^{-1}$ with the magnitude of the eddy diffusivity inversely proportional to the strength of interior potential vorticity gradients. This approach provided a distribution of eddy diffusivities as a function of streamline, or SSH contour, but did not allow for along-stream variations in mixing properties. Ferrari and Nikurashin (2010) updated this approach by showing that strong mean flows can suppress the rate of eddy mixing and reduce the magnitude of the eddy diffusivity. Qualitatively, Ferrari and Nikurashin (2010) argued that a strong mean flow can effectively advect tracers downstream on time scales that are fast compared to the time needed to erode tracer gradients by the background eddy field. Quantitatively, this study provided an expression for the magnitude of the eddy diffusivity that accounted for the local magnitude of EKE and the background mean flow, both obtained from satellite altimetry observations, and was validated against the effective diffusivity approach. Their map of eddy diffusivities in the Southern Ocean revised earlier estimates (Keffer and Holloway, 1988; Stammer, 1998) to show that the suppression of the eddy diffusivity only occurs outside of standing meanders (Fig. 12.3b). Naveira Garabato et al. (2011) and Roach et al. (2016) observationally estimated the eddy diffusivity from repeat hydrographic section and Argo float trajectories respectively, finding that in most regions, ACC jets suppress eddy diffusivities, but exceptions occur along transects near major bathymetric features – regions they labeled "leaky jets."

Progress on the quantification of an eddy diffusivity in the Southern Ocean coincided with a reevaluation of how to identify and classify Southern Ocean jets (Chapman, 2014). While altimetric observations provided a comprehensive view of the multiple-jet structure of the ACC (Sokolov and Rintoul, 2009), these were still defined as circumpolar features, linked to contours of SSH. Thompson et al. (2010), using model output from a high-resolution ocean simulation, argued that near topographic features, coherent jets break down but re-emerge further downstream. The regions of jet rearrangement were collocated with the

high EKE regions in the lee of topography. Both diagnosed eddy fluxes from idealized numerical simulations (MacCready and Rhines, 2001) as well as the advection of passive particles with satellite-derived surface velocities (Thompson and Sallée, 2012) offer evidence that standing meander regions are sites of enhanced meridional exchange. This finding has subsequently been supported by the analysis of cross-front transport of tracers and Lagrangian particles in high-resolution numerical models (Fig. 12.3c; Dufour et al., 2015; Tamsitt et al., 2017).

The previous discussion focused on mixing properties of the ACC, but mixing and stirring in the Southern Ocean's subpolar gyres and at the Antarctic margins are also critical as they regulate upwelling and downwelling branches of the overturning circulation's lower cell (Orsi et al., 1999; Gordon et al., 2001; Vernet et al., 2019). The two major Southern Hemisphere subpolar gyres, the Weddell and the Ross Gyres, are forced by a large-scale cyclonic wind-stress curl, and their interior dynamics follow Sverdrup balance in which a poleward flow is closed by equatorward western boundary currents (Gordon et al., 1981). Yet, these gyres are also distinct from their low-latitude counterparts. First, the subpolar gyres are strongly constrained by topography along their northern and southern boundaries, not just to east and west. Furthermore, these gyres participate in the global overturning circulation in ways that the subtropical and Northern Hemisphere subpolar gyres do not. In the gyres of the northern basins, most of the recirculation occurs above the thermocline and does not participate in the pole-to-pole overturning (Wolfe and Cessi, 2011). In contrast, the Southern Ocean subpolar gyres are the primary pathway by which volume and water mass properties are exchanged between the southern boundary of the ACC and Antarctica's continental shelf. The shelf is a site of strong water mass transformation processes, including the formation of AABW, which fuels the ocean's deep overturning (see following section). A new frontier in Southern Ocean research is the impact of mesoscale dynamics on both the long-term mean and variability of the subpolar gyres. Some of this work is influenced by Arctic studies: the Beaufort Gyre's mean density structure is set by eddy fluxes largely generated from boundary currents (Meneghello et al., 2017; Manucharyan and Spall, 2016). This process has also been highlighted in the Weddell Gyre as being key to setting gyre variability over seasonal to inter-annual timescales (Su et al., 2014). In Southern Ocean subpolar gyres, eddy generation is tightly linked to the dynamics of boundary currents over the continental shelf that also regulate heat transport toward Antarctica's floating ice shelves, although as the gyres' northern boundaries coincide with the ACC, lateral eddy fluxes are likely also critical for setting long-term properties (Roach and Speer, 2019).

The impact of gyre variability on the climate system relates to the ventilation of deep water masses, in particular in the Weddell Gyre, on interannual to seasonal time scales (Gordon et al., 2010). Variations in wind-stress curl have been hypothesized to vertically displace isopycnals in the gyre interior and modify the range of density classes that either incrop on topographic ridges to

the north of the gyre or permit an adiabatic pathway into the southern ACC (Meredith et al., 2008). Su et al. (2014) introduced an idealized model of a subpolar gyre, borrowing ideas from the residual mean theory developed in zonal channels. Similar to zonally symmetric geometries, both mean (wind-driven) and eddy circulations contribute to the density structure of the gyre. In the gyre interior, isopycnals are displaced vertically by surface Ekman pumping, which leads to modifications in lateral density gradients and associated mesoscale eddy buoyancy fluxes near the gyre boundary. Su et al. (2014) tested various parameterizations of mesoscale eddy diffusivity, in particular accounting for mixing suppression by topographic slopes (Isachsen, 2011), and found that eddy variability can explain moored observations of phasing in temperature and salinity over the continental slope in response to a seasonally varying wind stress (Gordon et al., 2010; Dotto et al., 2018).

The transport of heat around the subpolar gyres also impacts the delivery of warm water toward the margins of Antarctica and ultimately to the continental shelf where interactions with floating ice shelves and sea ice provide a closure of the overturning circulation. A key dynamical gateway for this poleward transport of heat is the continental shelf break, where topographic flow constraints over the shelf and slope combine with a strong frontal structure to establish the Antarctic Slope Front (ASF) and an associated along-slope current (Jacobs, 1991; Thompson et al., 2018). Traditionally, the exchange of heat and other tracers across the ASF was assumed to be dominated by Ekman transport in surface and bottom boundary layers (e.g. Gill, 1973), yet the advent of higher resolution observations from ship-based, autonomous, and instrumented seal data sets revealed that (i) the ASF is a turbulent and variable circulation feature and (ii) eddy fluxes are critical for closing momentum, buoyancy, and tracer budgets. In perhaps the earliest study to argue for the importance of eddy mixing at the Antarctic margins, Nøst et al. (2011) used an insightful combination of observations and high-resolution numerical modeling to show that the inflow of warm Circumpolar Deep Water across the Eastern Weddell Sea continental shelf break is dominated by eddy transport. The interplay between wind and eddy overturning circulations was examined more explicitly in an idealized zonally symmetric modeling framework by Stewart and Thompson (2013), who highlighted the suppression of eddy mixing over the continental slope (Isachsen, 2011). This study, as well as a subsequent analysis of glider data in the northwestern Weddell Sea (Thompson et al., 2014), argued that the eddy-induced onshore transport of CDW was due to eddy thickness fluxes, $\overline{v'h'}$ (see 12.1). The establishment of strong along-isopycnal temperature gradients due to the proximity of CDW and colder water masses on the shelf implies that eddy stirring can also contribute to the eddy heat flux. Indeed, Palóczy et al. (2018) found that stirring along isopycnal surfaces dominated the heat transport across the continental slope in a 0.1° coupled ocean–sea ice simulations. The importance of eddy transport is also supported by measurements from the West Antarctic Peninsula (WAP), which, due to its proximity to research stations and

a LTER (Long Term Ecological Research) program, has been well observed. Here, mesoscale eddies have emerged as the most prominent mechanism of heat delivery to the WAP shelf (Dinniman et al., 2011; Martinson and McKee, 2012; Brearley et al., 2019), in particular at Marguerite Trough where up to 50% of the lateral onshore heat transport of warm upper CDW to the WAP shelf was attributed to coherent eddies (Couto et al., 2017).

A consistent message from numerical simulations of the Antarctic margins is that resolution of scales smaller than the Rossby deformation radius on the shelf, typically less than 5 km, is required to fully represent eddy mixing and transport processes, (St-Laurent et al., 2013; Stewart and Thompson, 2015; Dinniman et al., 2016). Recent simulations, carried out over a short period of time but with an extremely high 1/48° resolution, indicate that for almost all regions around Antarctica, the total transport of heat across the shelf break is well described by the eddy component, although this remarkably arises from a near-complete cancellation between large mean-flow and tidal contributions to the heat transport (Stewart et al., 2018). Tidal and eddy contributions were delimited by time scales shorter than and longer than 1 day, respectively. While earlier studies have focused on wind forcing to explore modulation of mixing and eddy transport at the shelf break, recent studies have highlighted how shelf processes can modify frontal properties at the shelf break and feed back on cross-slope transport (Hattermann, 2018; Daae et al., 2020).

## 12.5 INTERIOR MIXING: CLOSING THE BUDGETS THROUGH TURBULENCE AT THE SMALLEST SCALES

### 12.5.1 Foundations

Isopycnals associated with the denser LCDW and AABW of the lower overturning branch (Fig. 12.1) do not outcrop in regions of positive surface buoyancy forcing. They instead rely on interior diabatic processes to converge buoyancy in the deep ocean, producing lighter waters that can upwell and return to the surface, as illustrated in Fig. 12.5 (Orsi et al., 1999, 2002; Naveira Garabato et al., 2007; Mashayek et al., 2015). Since AABW gradually flows northward forming the deepest component of the global overturning circulation (e.g. Johnson, 2008), without cross-density exchanges the global oceans would gradually fill up with cold dense waters, largely dissociated from the surface ocean and atmosphere. In this section we outline the dominant processes responsible for the diabatic return of the bottom waters of the Southern Ocean, and we discuss the critical role that abyssal Southern Ocean mixing may play in controlling the overturning circulation, thereby influencing the global climate system (see also Chapter 2).

### 12.5.2 Recent Findings: Sub-surface diapycnal mixing pathways in the Southern Ocean

The dissipation of wind, tidal, and geothermal energy powers interior mixing and abyssal diapycnal upwelling in the ocean. In the Southern Ocean, the energy input from internal tides and geothermal heat fluxes is weak compared to that from standing internal waves, or lee waves (de Lavergne et al., 2016). Lee waves, generated by the interaction of bottom flow with seabed topography, transport energy from the large-scale, wind-driven circulation to turbulent scales when they break, giving rise to diapycnal mixing in the ocean interior (Fig. 12.4; see also Chapter 6; Bell, 1975; Thorpe, 2005; Cusack et al., 2017). Of the ~1 TW of wind power that is transferred into geostrophic ocean currents globally (Wunsch, 1998; von Storch et al., 2007), a significant fraction, estimated between 0.15 TW and 0.75 TW, is transmitted into lee waves (Nikurashin and Ferrari, 2011; Scott et al., 2011; Wright et al., 2014; Melet et al., 2014; Trossman et al., 2016; Yang et al., 2018). Lee wave energy flux estimates are generated by applying linear lee wave theory (Bell, 1975) to global distributions of topographic roughness, near-bottom stratification, and current speeds. Importantly, approximately half of the total global lee wave energy flux occurs in the Southern Ocean where the strong deep flow and intense eddy activity of the ACC interact with regions of rough topography (Gille and Kelly, 1996). Lee waves, characterized by short vertical scales, tend to break close to their generation sites and dissipate within 1 km of the topography, making this process an important source of abyssal mixing (see Chapter 6; Nikurashin and Ferrari, 2010b,a). More refined estimates of the proportion of lee wave energy that dissipates locally is still an open question (Waterman et al., 2014; Kunze and Lien, 2019). The bottom-enhanced mixing signature associated with lee wave breaking is evident in depth profiles of turbulent dissipation within energetic regions of the ACC (Fig. 12.6d; see also St. Laurent et al., 2013; Waterman et al., 2013; Sheen et al., 2013).

Southern Ocean abyssal mixing is by no means spatially or temporally homogeneous. Mixing hotspots are found in regions characterized by rough topography and intense mesoscale eddy flow, particularly at frontal locations: exactly the conditions where one might expect enhanced lee wave generation. Further evidence of the role of lee wave activity in generating abyssal mixing in the Southern Ocean is provided by the measurement of vigorous, upward-propagating, sub-inertial internal wave energy at mixing hotspots (e.g. Waterman et al., 2013; Brearley et al., 2013; Sheen et al., 2013; Meyer et al., 2015, 2016). Such mixing hotspots include Kerguelen Plateau, Drake Passage and the Scotia Sea (Naveira Garabato et al., 2004; Sloyan, 2005; St. Laurent et al., 2013; Waterman et al., 2013; Meyer et al., 2015; Sheen et al., 2013). Thus, topographic features in the Southern Ocean shape surface mixing properties (section 12.3), cross-front transport in the interior (section 12.4), as well as deep diabatic mixing.

In addition to lee waves having patchy spatial distributions, they also show temporally variable radiation and breaking, as indicated by mooring and other

time-series data. This variability is due to changes in the strength and position of the background flow and to surface eddy activity over climatic timescales (Brearley et al., 2013; Sheen et al., 2014). Much of the observational evidence for the role of lee-wave-driven mixing in the Southern Ocean cited here is the output of two landmark field programs: the Southern Ocean FINEstructure (SOFINE) project and the Diapycnal and Isopycnal Mixing Experiment in the Southern Ocean (DIMES). See Case Study Box for an overview of the DIMES program.

The energy associated with breaking internal waves both produces heating through viscous dissipation, $\epsilon$, and changes the potential energy of the water column by mixing, represented by a turbulent buoyancy flux, $F_\rho = -(g/\rho_0)\overline{w'\rho'}$, where $g$ is the acceleration due to gravity, $\rho_0$ is the mean density, and $\overline{w'\rho'}$ is the time-averaged correlation between the vertical velocity and density fluctuations. These two energy pathways are related by the mixing efficiency, $\Gamma = F_\rho/\epsilon$, which is generally taken to be a constant equal to 0.2 (Gregg et al., 2018). The diapycnal velocity induced by a buoyancy flux, $w^*$, is related to both the vertical gradient of the turbulent buoyancy flux, $F_\rho$, and the vertical stratification, $N^2$, such that

$$w^* = -\frac{1}{N^2}\frac{\partial F_\rho}{\partial z} = -\frac{1}{N^2}\frac{\partial(\Gamma\epsilon)}{\partial z}. \tag{12.2}$$

Thus, for a constant mixing efficiency, a dissipation ($\epsilon$) profile that increases/decreases with depth acts to drive transport toward higher/lower densities (inset in Fig. 12.5; see also e.g. Polzin et al., 1997; St. Laurent et al., 2001; McDougall and Ferrari, 2017). On initial inspection, this relationship would suggest that the characteristic Southern Ocean bottom-intensified viscous dissipation associated with lee wave generation and breaking would result in an overall cross-density downwelling, rather than lightening LCDWs and bottom waters, as required to close the overturning circulation. One approach to resolving this apparent inconsistency is to assume that the mixing efficiency, $\Gamma$, decays to zero close to the ocean floor to satisfy a no density-flux boundary condition, $F_\rho = 0$ (Polzin et al., 1997; St. Laurent et al., 2001; Ferrari et al., 2016; de Lavergne et al., 2016); although turbulent dissipation, $\epsilon$, may be enhanced near the seabed, due to the weak stratification, here there can be little density flux, i.e. you cannot mix water that is already well-mixed. The result is a narrow turbulent boundary layer whereby $\Gamma\epsilon$ decreases with depth. The associated diapycnal flow, $w^*$, will act parallel to the boundary (since isopycnals will intersect the ocean floor at right angles due to the no-flux boundary condition), and water within the bottom boundary layer will cross to lighter density layers and upwell (Fig. 12.5). To assess the net abyssal diapycnal upwelling over basin scales, the shape of the ocean floor must be considered: the area of interaction between the seafloor and water of a particular density will determine the overall turbulent buoyancy flux experienced (de Lavergne et al., 2017; Holmes et al., 2018). Ferrari et al. (2016), for example, show that in numerical models the diapycnal upwelling of LCDW and AABW preferentially occurs where the associated density layers intersect

with continental margins and abyssal ridges. The resultant boundary layer upwelling is found to be sufficient to overcome the diapycnal downwelling within the stratified ocean interior and hence close the abyssal overturning circulation. Parameterized mixing calculations by de Lavergne et al. (2016) support these results, reporting that lee-waves in the Southern Ocean drive both upwelling of the bottom-most waters along topographic features and widespread downwelling in overlying water masses. Mashayek et al. (2017b) also challenged the assumption of a constant mixing efficiency above the bottom boundary layer, demonstrating that potential variations in $\Gamma$ result in a leading order difference to the abyssal branch of the overturning circulation. Despite recent progress in assessing the processes that drive upwelling in the Southern Ocean abyss, bottom boundary layer observations are scarce, and theories are still very much actively developing. We refer the reader to Chapter 7 for a comprehensive discussion of the current thinking on mixing at the ocean's bottom boundary.

Lee-wave-enhanced, near-boundary dissipation within the Southern Ocean also influences tracer distributions. The overall mixing experienced by a tracer is dependent not only on the geographic distribution of mixing, but also the proportion of time spent in regions of varying mixing intensities. By considering lateral advection, stirring and topographic steering of a tracer field, Mashayek et al. (2017a) showed that the tracer residency time spent in topographic mixing hotspots is enhanced in the Southern Ocean. This result explained the seemingly low values of observed 'snapshot' measurements of diapycnal mixing when compared to the time-averaged mixing experienced by a tracer (See the DIMES Case Study box for further details).

In addition to bottom-enhanced lee wave breaking, several other mechanisms have been reported as important contributors to subsurface diabatic motion in the Southern Ocean. These mechanisms include tidal boundary mixing and entrainment into plumes (Silvester et al., 2014; Orsi et al., 2002; Daae et al., 2019). Mixing can also be catalyzed by other near-boundary processes such as topographically generated submesoscale flows, as found by Ruan et al. (2017) and later linked to enhanced turbulent dissipation by Naveira Garabato et al. (2019), along the Antarctic continental slope, resulting in the transformation of LCDW into lighter water masses (see also Chapter 8). Klymak (2018) and Klymak et al. (2021) also highlighted the potential importance of turbulence generated by near-bottom flow over topographic scales too large to emit propagating internal waves. The blocking, steering and hydraulic effects associated with large topographic obstacles could represent a dominant pathway for the removal and dissipation of energy from the mean flow in the Southern Ocean. The inhomogeneous nature of interior mixing associated with large-amplitude topography (generally in the lee of large obstacles) presents a challenge to observational sampling.

In summary, a new picture is emerging of a complex pattern of abyssal mixing and tracer distribution within the Southern Ocean, set by the geography of both the stirring and steering of eddies and currents, and the topographically induced upwelling and interior downwelling in relation to water mass distribu-

tions. In particular, the processes outlined above could indicate a more vigorous connection or 'short-circuiting' between the upper and lower branches of the overturning circulation than previously thought (Naveira Garabato et al., 2007; McDougall and Ferrari, 2017; Mashayek et al., 2017b,a).

## 12.6 GRAND CHALLENGES

Targeted field campaigns and modeling studies of the past decade have substantially increased our understanding of turbulent processes in the Southern Ocean and of their impact on the Earth system as a whole. Despite recent advances, the processes that control the strength and pathways of the abyssal overturning, as well as the exchange between the upper and lower branches, remain unclear. Such knowledge gaps highlight the need for accurate mapping of both the spatial and the temporal variability of adiabatic mixing, and its driving processes, within the Southern Ocean. Field programs such as DIMES have been game-changers in advancing our understanding of Southern Ocean physics, both in terms of acquiring new measurements and in informing modeling studies (e.g. Tulloch et al., 2014; Chen et al., 2015; Ferrari et al., 2016). However, the remote, harsh conditions associated with the Southern Ocean, particularly during the winter months, make shipboard measurements challenging. Emerging technologies such as autonomous instrumentation, gliders and floats, along with international collaborative programs will likely play a vital role in better constraining Southern Ocean mixing (Meredith et al., 2013).

Here we identify a few priorities for future research directions, targeting specific processes, i.e. upper-ocean turbulence and watermass transformation, along-isopycnal adiabatic mixing, and interior mixing, and opportunities for probing links between these mixing processes to assess how the components of the system work together.

At the ocean surface, challenges center around sampling small-scale and intermittent processes. This includes finding ways to sample regional variations throughout the year to probe how Southern Ocean basin asymmetries and latitudinal differences (Sallée et al., 2010) contribute to spatial variations in ocean mixing. Key processes that require further study include the impact of waves and Langmuir circulation on air-sea exchange as well as mechanisms that govern property exchange between the mixed layer and the thermocline. In particular, GCM simulations typically have mixed layers that are shallower, fresher, and warmer than observations, resulting in a stronger density contrast between the mixed layer and the thermocline below that is likely to impede vertical exchange (Belcher et al., 2012; Sallée et al., 2013). The marginal ice zone presents its own challenges, and there is a specific need to explore the impact of sea ice on the upper ocean and to obtain direct mixing estimates within and under sea ice. Observations are necessary to improve and validate the representation of these processes in climate models, which have traditionally had significant biases in polar regions (Heuzé et al., 2013).

Deep-water mass conversion, especially along the bottom boundary, presents challenges that should receive as much attention as surface boundary layer turbulence. One challenge is that mixing associated with waves that break far away from their generation site, such as internal tides, makes tracking energy dissipation pathways difficult (Oka and Niwa, 2013; de Lavergne et al., 2016; Meyer et al., 2016). The recent work by Ferrari et al. (2016) suggests that a full picture of the abyssal circulation in the Southern Ocean will require detailed observations of turbulent boundary layer fluxes in the ocean abyss. Autonomous vehicles have already proven useful in identifying active submesoscale flows (Ruan et al., 2017) and enhanced diapycnal mixing (Naveira Garabato et al., 2019) over sloping topography in the Southern Ocean. The challenge to better understand Southern Ocean abyssal mixing requires a multi-pronged approach, including more observations, improved theory of mixing parameterizations and further modeling studies, and tapping into the specific mechanisms and insights detailed in other chapters of this book.

Improved observations, theory and models will feed into a more accurate mapping of the spatial patchiness and temporal evolution of interior and abyssal mixing in the Southern Ocean. Such developments will be key to determining the intricate water mass transport pathways within our oceans and the strength of the abyssal overturning. In particular setting the balance between topographically focused diapycnal upwelling and interior sinking will have implications for the diapycnal exchange of tracers and in turn ocean ventilation (Holmes et al., 2019), carbon storage and marine biogeochemical cycling. Indeed, model outputs are highly sensitive to differing spatial distributions of Southern Ocean wave-breaking energy with radically different implications for ocean circulation (Simmons et al., 2004; Saenko et al., 2012; Melet et al., 2014; Mashayek et al., 2015, 2017a).

A final challenge is to develop a physical understanding of mixing that acknowledges the links and feedbacks between different mixing processes. Here, a few examples highlight contributions that help build these connections.

- Naveira Garabato et al. (2016) used a small number of direct microstructure profiles to estimate the rates of both isopycnal and diapycnal (or isoneutral and dianeutral) mixing across the ACC as well as the magnitude of the overturning circulation. This study emphasized the sensitive link between small-scale mixing and the large-scale overturning that will have a significant impact on climate evolution in response to warming.
- Stewart and Hogg (2017) used an idealized numerical model with a topographic ridge to explore a similar link between smaller and larger scales. They showed that modification in AABW production on the continental shelf influences the outflow of this dense water across the ACC, which in turn modifies the density structure of the deep western boundary current on the downstream side of the topographic ridge and influences eddy fluxes. This change has a signature in the SSH field, suggesting the potential for monitoring

near-coast changes via altimetry in the future.
- Finally, Dufour et al. (2017) completed centennial-scale global simulations under pre-industrial forcing at two resolutions. The high-resolution (0.1°) simulation produced intermittent polynyas in the Weddell Sea, while the coarser resolution simulation did not.

All of these studies offer insight into the sensitive balance between small-scale processes and large-scale circulations in the Southern Ocean, and they suggest approaches that should be further explored in future research. Understanding these interactions over decadal-to-centennial timescales is a critical challenge for the accurate prediction of future climate. Improvements in physical understanding and model representations of Southern Ocean mixing will directly impact the fidelity of projections for future ocean heat and carbon storage as well as the structure and strength of the MOC in different climate regimes.

## DIMES CASE STUDY BOX

### Foundations

DIMES (The Diapycnal and Isopycnal Mixing Experiment in the Southern Ocean) was an extensive UK/US field program aimed at quantifying both the cross-density (diapycnal) and along density (isopycnal) mixing in the Southern Ocean. The project's motivation stemmed from a severe lack of *in situ* observations of Southern Ocean mixing and its driving processes, crucial to understanding the strength and structure of both the upper and lower limbs of the MOC. DIMES was located in the eastern Pacific and western Atlantic sectors of the ACC, providing a comparison of the mixing in two contrasting regions: the more quiescent, smooth-bottomed southeast Pacific; and the energetic Drake Passage and Scotia Sea, characterized by vigorous mesoscale eddy flow and rough topography (Fig. 12.6a).

The backbone of the DIMES program was a tracer release experiment. A parcel of inert, non-natural chemical $CF_3SF_5$ was released along a density surface at a depth of 1300 m in the southeast Pacific in 2009. Following the release, annual research cruises between 2009 and 2013 were scheduled to track the advection of the tracer as it progressed downstream through Drake Passage and the Scotia Sea as well as its subsequent dispersal in both along and across density surfaces. The cross-density spread of the tracer was measured at multiple locations during each cruise, from which the mean diapycnal diffusivity experienced along the tracer path since its release could be computed (Ledwell et al., 2011; Watson et al., 2014). A total of 210 isopycnal-following "RAFOS" floats, tracked using acoustic sound sources, were deployed to evaluate along-isopycnal stirring and mixing processes (LaCasce et al., 2014; Balwada et al., 2016). Vertical profiles of "on the spot" turbulent dissipation rates, $\epsilon$, were also collected using microstructure profilers or VMPs (Fig. 12.6b; Chapter 14). VMPs capture high-resolution (cm scale) vertical measurements of velocity shear, from which

spectra can be computed and directly compared with turbulent theory via the Batchelor (1959) spectrum to extract dissipation rates. In DIMES, microstructure turbulence observations were complemented with co-located measurements of the kinetic and potential energy of internal waves. Internal wave energy was extracted from velocity shear and strain spectra, computed from finescale vertical measurements, $O$(1-100 m), of horizontal current flow, temperature and salinity, as recorded by LADCP and CTD instruments. Moreover the direction of lee wave propagation and characteristic frequency content can be deduced from such data (e.g. Waterman et al., 2014). Finescale measurements are too coarse to capture small-scale turbulent motions directly; however, $\epsilon$, may be derived from internal wave energy spectra using finescale parameterizations (Polzin et al., 1995). Although approximate, the finescale parameterization method is powerful as it enables cross-density mixing to be deduced from plentiful (and historical) hydrographic data as collected from CTDs (as opposed to scarce and difficult to obtain direct microstructure observations). In addition to tracer, floats, and microstructure, the DIMES experiment included a plethora of other observation platforms including a two-year mooring array in Drake Passage (Brearley et al., 2013), EM-APEX floats (Kilbourne and Girton, 2015), and targeted deployment of eXpendable CTDs to assess turbulence proxies (Frants et al., 2013).

## Key Results

The DIMES data have fed into a range of both observational and modeling studies, many of which have been outlined in this chapter. Here we cover the key findings in relation to subsurface diapycnal and isopycnal mixing observational studies. Both tracer release and direct turbulence measurements from microstructure profiles showed an order of magnitude increase (estimates of turbulent dissipation, $\epsilon$, ranged from $10^{-10}$ to $10^{-9}$ W kg$^{-1}$) in deep mixing between the southeast Pacific and southwest Atlantic (Fig. 12.6c,d; St. Laurent et al., 2013; Watson et al., 2014; Sheen et al., 2013). These results support the dominant role that topographically generated lee waves play in driving turbulent dissipation in the Southern Ocean. In addition, higher mixing rates were found to be associated with enhanced bottom currents, such as at frontal locations (St. Laurent et al., 2013; Brearley et al., 2013; Sheen et al., 2013). Mixing hotspots typically displayed enhanced turbulent dissipation within the bottom 1 km of the ocean, a characteristic signal of the topographic generation and breaking of internal waves (Fig. 12.6d). Mixing rates were also found to be modified by interior mesoscale features (Sheen et al., 2015).

Finescale measurements indicated that regions of enhanced mixing were associated with more energetic, relatively high-frequency internal waves that propagate away from the seafloor. In comparison, the upper ocean internal wave field was composed of downward propagating, near-inertial energy, characteristic of surface generated wind-driven waves (Sheen et al., 2013; Brearley et al., 2013). The DIMES data also supported other studies in that although lee wave energy

flux calculations and finescale estimations of mixing are generally consistent with direct turbulent measurements (see Chapter 6), they can over-predict the mixing measured directly with microstructure profilers under certain conditions, and hence parameterization theory needs refinement (Frants et al., 2013; Waterman et al., 2013, 2014; Sheen et al., 2013; Takahashi and Hibiya, 2019).

DIMES was unprecedented in the number of microstructure profiles that were collected in the Southern Ocean (> 75). However, measurements still fell short of capturing the full picture of abyssal mixing due to its spatial and temporal variability. Finescale parameterizations help to fill in the sampling gap. For example, the DIMES mooring array, which was deployed for a year in Drake Passage, and the repeat Drake Passage hydrographic section SR1B, which has been sampled annually since 1993, were used to show that Southern Ocean abyssal mixing is dependent on surface eddy energy and hence potentially climatic perturbations in wind forcing (Sheen et al., 2014). Another approach to fill observational data gaps of abyssal mixing is through numerical model runs informed by observations. Mashayek et al. (2017a) used a high-resolution ocean model to resolve an apparent inconsistency uncovered by DIMES: the cross-density mixing required for the observed vertical spreading of the DIMES tracer was an order of magnitude higher than that recorded by microstructure measurements of mixing at the mean tracer depth in regions of rough topography. The model showed that efficient tracer stirring and the long residency time spent by the tracer in stratified, near-boundary strong mixing hotspots explained the large diapycnal diffusivities experienced by the tracer. It was found that geostrophic eddies and the mean flow tend to stir and trap the tracer near topography. The impact of uneven residency times in regions of high mixing on the tracer spread could not have been captured by spot microstructure measurements.

DIMES isopycnal mixing studies explored the hypothesis that the effective lateral diffusivity is small in the core of the ACC and enhanced at the "steering level," where the westward propagation of Rossby waves is balanced by the eastward advection of the ACC (Smith and Marshall, 2009). Modeling studies, completed early in the project, highlighted considerable nuance in the spatio-temporal patterns of eddy mixing (e.g. Griesel et al., 2009, 2010; Abernathey et al., 2010; Klocker et al., 2012). To assess the effect of the mean flow on the vertical structure of lateral diffusivity, floats were targeted to drift at two depths, ~700 m and ~1800 m, with the tracer near 1300 m. Float observations implied a large range of effective eddy diffusivity values in the southeast Pacific that ranged from 2800±600 $m^2\ s^{-1}$ at 700 m depth to 990±200 $m^2\ s^{-1}$ at 1800 m depth. Even lower values were associated with cross-ACC diffusivity estimates, which were suppressed at shallower levels (690±150 $m^2\ s^{-1}$ at 700 m depth as compared to 1000±200 $m^2\ s^{-1}$ at 1800 m depth), consistent with theoretical predictions (LaCasce et al., 2014; Balwada et al., 2016). Notably, this signal of a mid-depth maximum in cross-ACC eddy diffusivity emerged at time scales greater than 6 months, which is significantly longer than the integral time scale of $O$(10 days). An assessment of the tracer spread suggested a comparable

diffusivity: 710±260 $m^2\ s^{-1}$ (Tulloch et al., 2014). Finally, in the more energetic Scotia Sea, the cross-ACC diffusivity was larger, 1200±500 $m^2\ s^{-1}$ (Balwada et al., 2016).

In addition to estimating the mesoscale lateral eddy diffusivity, studies also characterized eddy stirring at scales smaller than the dominant eddy scales ($\sim$ 100 km). A much smaller eddy diffusivity, roughly 20 $m^2\ s^{-1}$, was estimated at scales of $\sim$10 km (Boland et al., 2015; Balwada et al., 2021). Assessing the physical processes that give rise to these diffusivity values, Zika et al. (2020) and Balwada et al. (2021) argued that the eddy stirring at mid-depth in this region of the ACC is likely non-local, such that the largest eddies are primarily responsible for stirring and filamenting the tracers (Garrett, 1983).

## ACKNOWLEDGMENTS

STG acknowledges support from the U.S. National Science Foundation (NSF Grants PLR-1425989, OCE-1658001, and OPP-1936222). KS was supported by the UK National Environmental Research Council (NERC) for her work on the DIMES project. SS was supported by the Swedish Research Council (VR 2019-04400) and a Wallenberg Academy Fellowship (WAF 2015.0186). AFT acknowledges support from the U.S. National Science Foundation (NSF Grants OCE-1756956, OPP-1644172, OPP-2023259). We are grateful to Kevin Speer, Dhruv Balwada and an anonymous reviewer for comments that improved this chapter.

## SHORT BIOS OF AUTHORS

- Sarah T. Gille is a professor of physical oceanography at Scripps Institution of Oceanography, University of California, San Diego. Previously, she completed her PhD in the MIT/Woods Hole Oceanographic Institution Joint Program, carried out postdocs at Scripps Institution of Oceanography and at the University of East Anglia, and served on the faculty of the University of California Irvine.
- Katy Sheen is a senior lecturer in physical geography at the University of Exeter. Before taking up her current position, she completed a PhD at the University of Cambridge and a postdoc at the University of Southampton, and worked as a senior scientist at the UK Met Office Hadley Centre.
- Sebastiaan Swart is an associate professor of physical oceanography at the University of Gothenburg, Sweden, where he is currently a Wallenberg Academy Fellow. He also holds the title of Honorary Research Associate at the U. Cape Town, S. Africa. He received his PhD jointly from the University of Cape Town and the Université de Bretagne and was a postdoc and scientist at the South African Council for Scientific & Industrial Research.
- Andrew F. Thompson is a professor of Environmental Science & Engineering at the California Institute of Technology. He completed a PhD at Scripps

Institution of Oceanography, University of California San Diego, and was a postdoc at the University of East Anglia, the University of Cambridge, and the British Antarctic Survey.

Abernathey, R., Cessi, P., 2014. Equilibration of circumpolar currents with and without topography. J. Phys. Oceanogr. 44, 2107 – 2126.

Abernathey, R., Ferreira, D., 2015. Southern Ocean isopycnl mixing and ventilation changes driven by winds. Geophys. Res. Lett. 42, 10357–10365.

Abernathey, R., Marshall, J., Mazloff, M., Shuckburgh, E., 2010. Enhancement of mesoscale eddy stirring at steering levels in the Southern Ocean. J. Phys. Oceanogr. 40, 170–184. doi:10.1175/2009JPO4201.1.

Abernathey, R.P., Cerovecki, I., Holland, P.R., Newsom, E., Mazloff, M., Talley, L.D., 2016. Water-mass transformation by sea ice in the upper branch of the Southern Ocean overturning. Nature Geoscience 9, 596–601. doi:10.1038/ngeo2749.

Adams, K.A., Hosegood, P., Taylor, J.R., Sallée, J.B., Bachman, S., Torres, R., Stamper, M., 2017. Frontal circulation and submesoscale variability during the formation of a Southern Ocean mesoscale eddy. Journal of Physical Oceanography 47, 1737–1753. doi:10.1175/JPO-D-16-0266.1.

Akitomo, K., 1999. Open-ocean deep convection due to thermobaricity: 1. scaling argument. J. Geophysical Research 104, 5225–5234. doi:10.1029/1998JC900058.

Alford, M.H., MacKinnon, J.A., Simmons, H.L., Nash, J.D., 2016. Near-inertial internal gravity waves in the ocean. Annual Review of Marine Science 8, 95–123. doi:10.1146/annurev-marine-010814-015746.

Armour, K.C., Marshall, J., Scott, J.R., Donohoe, A., Newsom, E.R., 2016. Southern Ocean warming delayed by circumpolar upwelling and equatorward transport. Nature Geoscience 9, 549–554. doi:10.1038/ngeo2731.

Bachman, S.D., Klocker, A., 2020. Interaction of jets and submesoscale dynamics leads to rapid ocean ventilation. Journal of Physical Oceanography 50, 2873 – 2883. doi:10.1175/JPO-D-20-0117.1.

Bachman, S.D., Taylor, J.R., Adams, K.A., Hosegood, P.J., 2017. Mesoscale and submesoscale effects on mixed layer depth in the Southern Ocean. Journal of Physical Oceanography 47, 2173–2188. doi:10.1175/JPO-D-17-0034.1.

Balwada, D., LaCasce, J.H., Speer, K.G., Ferrari, R., 2021. Relative dispersion in the Antarctic Circumpolar Current. J. Phys. Oceanogr. 51, 553–574.

Balwada, D., Smith, K.S., Abernathey, R., 2018. Submesoscale vertical velocities enhance tracer subduction in an idealized Antarctic Circumpolar Current. Geophysical Research Letters 45, 9790–9802. doi:10.1029/2018GL079244.

Balwada, D., Speer, K.G., LaCasce, J.H., Owens, W.B., Marshall, J., Ferrari, R., 2016. Circulation and stirring in the southeast Pacific Ocean and the Scotia Sea sectors of the Antarctic Circumpolar Current. Journal of Physical Oceanography 46, 2005–2027. doi:10.1175/JPO-D-15-0207.1.

Barthel, A., Hogg, A.M., Waterman, S., Keating, S., 2017. Jet-topography interactions affect energy pathways to the deep Southern Ocean. J. Phys. Oceanogr. 47, 1799–1816.

Batchelor, G.K., 1959. Small-scale variation of convected quantities like temperature in turbulent fluid Part 1. General discussion and the case of small conductivity. Journal of Fluid Mechanics 5, 113–133. doi:10.1017/S002211205900009X.

Bebieva, Y., Speer, K., 2019. The regulation of sea ice thickness by double-diffusive processes in the Ross Gyre. Journal of Geophysical Research 184, 7068–7081. doi:10.1029/2019JC015247.

Belcher, S.E., Grant, A.L.M., Hanley, K.E., Fox-Kemper, B., Van Roekel, L., Sullivan, P.P., Large,

W.G., Brown, A., Hines, A., Calvert, D., Rutgersson, A., Pettersson, H., Bidlot, J.R., Janssen, P.A.E.M., Polton, J.A., 2012. A global perspective on Langmuir turbulence in the ocean surface boundary layer. Geophysical Research Letters 39. doi:10.1029/2012GL052932.

Bell, Jr., T.H., 1975. Topographically generated internal waves in the open ocean. Journal of Geophysical Research 80, 320–327. doi:10.1029/JC080i003p00320.

Biddle, L.C., Swart, S., 2020. The observed seasonal cycle of submesoscale processes in the Antarctic Marginal Ice Zone. Journal of Geophysical Research: Oceans 125, e2019JC015587. doi:10.1029/2019JC015587.

Bischoff, T., Thompson, A.F., 2014. Configuration of a Southern Ocean storm track. J. Phys. Oceanogr. 44, 3072–3078.

Boé, J., Hall, A., Qu, X., 2009. Deep ocean heat uptake as a major source of spread in transient climate change simulations. Geophys. Res. Lett 36. doi:10.1029/2009GL040845. l22791.

Boland, E.J.D., Shuckburgh, E., Haynes, P.H., Ledwell, J.R., Messias, M.J., Watson, A.J., 2015. Estimating a submesoscale diffusivity using a roughness measure applied to a tracer release experiment in the Southern Ocean. J. Phys. Oceanogr. 45, 247–257.

Bracco, A., Pedlosky, J., 2003. Vortex generation by topography in locally unstable baroclinic flows. J. Phys. Oceanogr. 33, 207–219.

Brearley, J.A., Moffat, C., Venables, H.J., Meredith, M.P., Dinniman, M.S., 2019. The role of eddies and topography in the export of shelf waters from the West Antarctica Peninsula shelf. J. Geophys. Res. .

Brearley, J.A., Sheen, K.L., Naveira Garabato, A.C., Smeed, D.A., Waterman, S., 2013. Eddy-induced modulation of turbulent dissipation over rough topography in the Southern Ocean. Journal of Physical Oceanography 43, 2288–2308. doi:10.1175/JPO-D-12-0222.1.

Caldeira, K., Duffy, P.B., 2000. The role of the Southern Ocean in uptake and storage of anthropogenic carbon dioxide. Science 287, 620–622. doi:10.1126/science.287.5453.620.

Campbell, E.C., Wilson, E.A., Moore, G.W.K., Riser, S.C., Brayton, C.E., Mazloff, M.R., Talley, L.D., 2019. Antarctic offshore polynyas linked to Southern Hemisphere climate anomalies. Nature 570, 319–325. doi:10.1038/s41586-019-1294-0.

Carranza, M.M., Gille, S.T., 2015. Southern Ocean wind-driven entrainment enhances satellite chlorophyll-a through the summer. Journal of Geophysical Research: Oceans 120, 304–323. doi:10.1002/2014JC010203.

Chapman, C.C., 2014. Southern Ocean jets and how to find them: Improving and comparing common jet detection methods. J. Geophys. Res. Oceans 119, 4318–4339.

Chapman, C.C., Hogg, A.M., Kiss, A.E., Rintoul, S.R., 2015. The dynamics of Southern Ocean storm tracks. J. Phys. Oceanogr. 45, 884–903.

Chen, R., Gille, S.T., McClean, J.L., Flierl, G.R., Griesel, A., 2015. A multiwavenumber theory for eddy diffusivities and its application to the southeast Pacific (DIMES) region. Journal of Physical Oceanography 45, 1877–1896. doi:10.1175/JPO-D-14-0229.1.

Chereskin, T.K., Donohue, K.A., D. R. Watts, K.L.T., Firing, Y.L., Cutting, A.L., 2009. Strong bottom currents and cyclogenesis in Drake Passage. Geophys. Res. Lett. 36.

Cisewski, B., Strass, V., Prandke, H., 2005. Upper-ocean vertical mixing in the Antarctic Polar Front Zone. Deep Sea Research Part II: Topical Studies in Oceanography 52, 1087–1108. doi:10.1016/j.dsr2.2005.01.010.

Couto, N., Martinson, D.G., Kohut, J., Schofield, O., 2017. Distribution of Upper Circumpolar Deep Water on the warming continental shelf of the West Antarctic Peninsula. J. Geophys. Res. Oceans 122, 5306–5315.

Cusack, J.M., Naveira Garabato, A.C., Smeed, D.A., Girton, J.B., 2017. Observation of a large lee wave in the Drake Passage. Journal of Physical Oceanography 47, 793–810. doi:10.1175/JPO-

D-16-0153.1.

Daae, K., Fer, I., Darelius, E., 2019. Variability and mixing of the Filchner Overflow Plume on the continental slope, Weddell Sea. J. Phys. Oceanogr. 49, 3–20.

Daae, K., Hattermann, T., Darelius, E., Mueller, R., Naughten, K.A., Timmermann, R., Hellmer, H.H., 2020. Necessary conditions for warm inflow towards the Filchner Ice Shelf, Weddell Sea. Geophys. Res. Lett. , in review.

Danabasoglu, G., McWilliams, J.C., 1995. Sensitivity of the global ocean circulation to parameterizations of mesoscale tracer transports. J. Climate 8, 2967–2987.

Danabasoglu, G., McWilliams, J.C., Gent, P.R., 1994. The role of mesoscale tracer transports in the global ocean circulation. Science 264, 1123–1126.

deSzoeke, R.A., Levine, M.D., 1981. The advective flux of heat by mean geostrophic motions in the Southern Ocean. Deep Sea Res. 28, 1057–1085.

DeVries, T., Primeau, F., 2011. Dynamically and observationally constrained estimates of water-mass distributions and ages in the global ocean. Journal of Physical Oceanography 41, 2381 – 2401. doi:10.1175/JPO-D-10-05011.1.

Dinniman, M.S., Asay-Davis, X.S., Galton-Fenzi, B.K., Holland, P.R., Jenkins, A., Timmermann, R., 2016. Modeling ice shelf/ocean interaction in Antarctica: A review. Oceanography 29, 144–153.

Dinniman, M.S., Klinck, J.M., Jr., W.O.S., 2011. A model study of Circumpolar Deep Water on the West Antarctic Peninsula and Ross Sea continental shelves. Deep Sea Res. II 58, 1508–1523.

Dong, S., Sprintall, J., Gille, S.T., Talley, L., 2008. Southern Ocean mixed-layer depth from Argo float profiles. J. Geophys. Res. 113. C06013, doi:10.1029/2006JC004051.

Dotto, T.S., Naveira Garabato, A., Bacon, S., Tsamados, M., Holland, P.R., Hooley, J., Frajka-Williams, E., Ridout, A., Meredith, M.P., 2018. Variability of the Ross Gyre, Southern Ocean: Drivers and responses revealed by satellite altimetry. Geophysical Research Letters 45, 6195–6204. doi:10.1029/2018GL078607.

Dufour, C.O., Griffies, S.M., de Souza, G.F., Frenger, I., Morrison, A.K., Palter, J.B., Sarmiento, J.L., Galbrait, E.D., Dunne, J.P., Anderson, W.G., Slater, R.D., 2015. Role of mesoscale eddies in cross-frontal transport of heat and biogeochemical tracers in the southern ocean. J. Phys. Oceanogr. , in press.

Dufour, C.O., Morrison, A.K., Griffies, S.M., Frenger, I., Zanowski, H., Winton, M., 2017. Preconditioning of the Weddell Sea polynya by the ocean mesoscale and dense water overflows. J. Climate 30, 7719–7737.

Erickson, Z.K., Thompson, A.F., Callies, J., Yu, X., Naveira Garabato, A., Klein, P., 2020. The vertical structure of open-ocean submesoscale variability during a full seasonal cycle. Journal of Physical Oceanography 50, 145–160. doi:10.1175/JPO-D-19-0030.1.

Ferrari, R., Mashayek, A., McDougall, T.J., Nikurashin, M., Campin, J.M., 2016. Turning ocean mixing upside down. Journal of Physical Oceanography 46, 2239–2261. doi:10.1175/JPO-D-15-0244.1.

Ferrari, R., Nikurashin, M., 2010. Suppression of eddy mixing diffusivity across jets in the Southern Ocean. J. Phys. Oceanogr. 40, 1501–1519.

Fons, S.W., Kurtz, N.T., 2019. Retrieval of snow freeboard of Antarctic sea ice using waveform fitting of CryoSat-2 returns. The Cryosphere 13, 861–878. doi:10.5194/tc-13-861-2019.

Forryan, A., Naveira Garabato, A.C., Polzin, K.L., Waterman, S., 2015. Rapid injection of near-inertial shear into the stratified upper ocean at an antarctic circumpolar current front. Geophysical Research Letters 42, 3431–3441. doi:10.1002/2015GL063494.

Fox-Kemper, B., Ferrari, R., Hallberg, R., 2008. Parameterization of Mixed Layer Eddies. Part I: Theory and Diagnosis. Journal of Physical Oceanography 38, 1145–1165.

doi:10.1175/2007JPO3792.1.

Frants, M., Damerell, G.M., Gille, S.T., Heywood, K.J., MacKinnon, J., Sprintall, J., 2013. An assessment of density-based finescale methods for estimating diapycnal diffusivity in the Southern Ocean. Journal of Atmospheric and Oceanic Technology 30, 2647–2661. doi:10.1175/JTECH-D-12-00241.1.

Fukamachi, Y., Rintoul, S.R., Church, J.A., Aoki, S., Sokolov, S., Rosenberg, M.A., Wakatsuchi, M., 2010. Strong export of Antarctic Bottom Water east of the Kerguelen Plateau. Nat. Geosci. 3, 327–331.

Garrett, C., 1983. On the initial streakness of a dispersing tracer in two-and three-dimensional turbulence. Dynam. Atmos. Oceans 7, 265–277.

Gent, P.R., 2016. Effects of Southern Hemisphere wind changes on the meridional overturning circulation in ocean models. Annual Review of Marine Science 8, 79–94. doi:10.1146/annurev-marine-122414-033929.

Gent, P.R., McWilliams, J.C., 1990. Isopycnal mixing in ocean circulation models. J. Phys. Oceanogr. 20, 150–155.

Giddy, I., Swart, S., du Plessis, M.D., Thompson, A.F., Nicholson, S.A., 2021. Stirring of sea-ice meltwater enhances submesoscale fronts in the Southern Ocean. Journal of Geophysical Research: Oceans doi:10.1029/2020JC016814.

Gill, A.E., 1973. Circulation and bottom water production in the Weddell Sea. Deep-Sea Res. 20, 111–140.

Gille, S.T., 2003. Float observations of the Southern Ocean: Part 2, Eddy fluxes. J. Phys. Oceanogr. 33, 1182–1196.

Gille, S.T., Kelly, K.A., 1996. Scales of spatial and temporal variability in the Southern Ocean. J. Geophys. Res. 101, 8759–8773.

Gille, S.T., McKee, D.C., Martinson, D.G., 2016. Temporal changes in the Antarctic Circumpolar Current: Implications for the Antarctic continental shelves. Oceanography 29. doi:10.5670/oceanog.2016.102.

Gordon, A.L., 1978. Deep Antarctic convection west of Maud Rise. Journal of Physical Oceanography 8, 600–612. doi:10.1175/1520-0485(1978)008<0600:DACWOM>2.0.CO;2.

Gordon, A.L., Huber, B., McKee, D., Visbeck, M., 2010. A seasonal cycle in the export of bottom water from the Weddell Sea. Nat. Geosci. 3, 551–556.

Gordon, A.L., Martinson, D.G., Taylor, H.W., 1981. The wind-driven circulation in the Weddell-Enderby Basin. Deep Sea Res. 28, 151–163.

Gordon, A.L., Visbeck, M., Huber, B., 2001. Export of Weddell Sea deep and bottom water. J. Geophys. Res. 106, 9005–9017.

Gregg, M., D'Asaro, E., Riley, J., Kunze, E., 2018. Mixing efficiency in the ocean. Annual Review of Marine Science 10, 443–473. doi:10.1146/annurev-marine-121916-063643.

Griesel, A., Gille, S.T., Sprintall, J., McClean, J.L., LaCasce, J.H., Maltrud, M.E., 2010. Isopycnal diffusivities in the Antarctic Circumpolar Current inferred from Lagrangian floats in an eddying model. J. Geophys. Res. 115. C06006, doi:10.1029/2009JC005821.

Griesel, A., Gille, S.T., Sprintall, J., McClean, J.L., Maltrud, M.E., 2009. Assessing eddy heat flux and its parameterization: A wavenumber perspective from a 1/10° ocean simulation. Ocean Modelling 29, 248–260.

Griffies, S.M., 1998. The Gent–McWilliams skew flux. Journal of Physical Oceanography 28, 831 – 841. doi:10.1175/1520-0485(1998)028<0831:TGMSF>2.0.CO;2.

Gruber, N., Landschützer, P., Lovenduski, N.S., 2019. The variable Southern Ocean carbon sink. Annual Review of Marine Science 11, 159–186. doi:10.1146/annurev-marine-121916-063407.

Hallberg, R., Gnanadesikan, A., 2006. The role of eddies in determining the structure and response

of the wind-driven Southern Hemisphere overturning: Results from the Modeling Eddies in the Southern Ocean (MESO) project. J. Phys. Oceanogr. 36, 2232–2252.

Hattermann, T., 2018. Antarctic thermocline dynamics along a narrow shelf with easterly winds. Journal of Physical Oceanography 48, 2419–2443. doi:10.1175/JPO-D-18-0064.1.

Haumann, A., Gruber, N., Münnich, M., Frenger, I., Kern, S., 2016. Sea-ice transport driving Southern Ocean salinity and its recent trends. Nature 537, 89–92. doi:doi.org/10.1038/nature1910.

Heuzé, C., Heywood, K.J., Stevens, D.P., Ridley, J.K., 2013. Southern Ocean bottom water characteristics in CMIP5 models. Geophys. Res. Lett. 40, 1409–1414.

Heywood, K.J., Schmidtko, S., Heuzé, C., Kaiser, J., Jickells, T.D., Queste, B.Y., Stevens, D.P., Wadley, M., Thompson, A.F., Fielding, S., Guihen, D., Creed, E., Ridley, J.K., Smith, W., 2014. Ocean processes at the Antarctic continental slope. Philosophical transactions. Series A, Mathematical, physical, and engineering sciences 372, 20130047. doi:10.1098/rsta.2013.0047.

Hogg, A.M.C., Meredith, M.P., Blundell, J.R., Wilson, C., 2008. Eddy heat flux in the Southern Ocean: Response to variable wind forcing. Journal of Climate 21, 608–620. doi:10.1175/2007JCLI1925.1.

Holland, D.M., 2001. Explaining the Weddell Polynya - a large ocean eddy shed at Maud Rise. Science 292, 1697–1700. doi:10.1126/science.1059322.

Holmes, R.M., de Lavergne, C., McDougall, T.J., 2018. Ridges, seamounts, troughs, and bowls: Topographic control of the dianeutral circulation in the abyssal ocean. Journal of Physical Oceanography 48, 861 – 882. doi:10.1175/JPO-D-17-0141.1.

Holmes, R.M., Zika, J.D., Ferrari, R., Thompson, A.F., Newom, E.R., England, M.H., 2019. Atlantic Ocean heat transport enabled by Indo-Pacific heat uptake and mixing. Geophys. Res. Lett. 46, 13939–13949.

Holte, J., Talley, L.D., Gilson, J., Roemmich, D., 2017. An Argo mixed layer climatology and database. Geophysical Research Letters 44, 5618–5626. doi:10.1002/2017GL073426.

Holte, J.W., Talley, L.D., Chereskin, T.K., Sloyan, B.M., 2012. The role of air-sea fluxes in Subantarctic Mode Water formation. Journal of Geophysical Research: Oceans 117. doi:10.1029/2011JC007798.

Huber, M.B., Zanna, L., 2017. Drivers of uncertainty in simulated ocean circulation and heat uptake. Geophysical Research Letters 44, 1402–1413. doi:10.1002/2016GL071587. 2016GL071587.

Hughes, C.W., Ash, E., 2001. Eddy forcing of the mean flow of the Southern Ocean. J. Geophys. Res. 106, 2713–2722.

Isachsen, P.E., 2011. Baroclinic instability and eddy tracer transport across sloping bottom topography: How well does a modified Eady model do in primitive equation simulations? Ocean Modell. 39, 183–199.

Ivchenko, V.O., Richards, K.J., Stevens, D.P., 1996. The Dynamics of the Antarctic Circumpolar Current. Journal of Physical Oceanography 26, 753–774. doi:10.1175/1520-0485(1996)026<0753:TDOTAC>2.0.CO;2.

Jacobs, S.S., 1991. On the nature and significance of the Antarctic Slope Front. Mar. Chem. 35, 9–24.

Jing, Z., Wu, L., Li, L., Liu, C., Liang, X., Chen, Z., Hu, D., Liu, Q., 2011. Turbulent diapycnal mixing in the subtropical northwestern Pacific: Spatial-seasonal variations and role of eddies. Journal of Geophysical Research: Oceans 116. doi:10.1029/2011JC007142.

Johnson, G.C., 2008. Quantifying Antarctic Bottom Water and North Atlantic Deep Water volumes. Journal of Geophysical Research: Oceans 113. doi:10.1029/2007JC004477.

Johnson, G.C., Bryden, H.L., 1989. On the size of the Antarctic Circumpolar Current. Deep Sea Res. 36, 39–53.

Johnson, L., Lee, C.M., D'Asaro, E.A., 2016. Global estimates of lateral springtime restratification.

Journal of Physical Oceanography 46, 1555–1573. doi:10.1175/JPO-D-15-0163.1.

Jouanno, J., Capet, X., Madec, G., Roullet, G., Klein, P., 2016. Dissipation of the energy imparted by mid-latitude storms in the Southern Ocean. Ocean Sciences 12, 743–769. doi:10.5194/os-12-743-2016.

Keffer, T., Holloway, G., 1988. Estimating Southern Ocean eddy flux of heat and salt from satellite altimetry. Nature 332, 624–626.

Kilbourne, B.F., Girton, J.B., 2015. Quantifying high-frequency wind energy flux into near-inertial motions in the southeast Pacific. Journal of Physical Oceanography 45, 369–386. doi:10.1175/JPO-D-14-0076.1.

Klein, P., Lapeyre, G., Large, W.G., 2004. Wind ringing of the ocean in presence of mesoscale eddies. Geophysical Research Letters 31. doi:10.1029/2004GL020274.

Klocker, A., 2018. Opening the window to the Southern Ocean: The role of jet dynamics. Science Advances 4. doi:10.1126/sciadv.aao4719.

Klocker, A., Ferrari, R., LaCasce, J., Merrifield, S., 2012. Reconciling float-based and tracer-based estimates of eddy diffusivities. J. Mar. Res. Submitted.

Klymak, J.M., 2018. Nonpropagating form drag and turbulence due to stratified flow over large-scale abyssal hill topography. Journal of Physical Oceanography 48, 2383–2395. doi:10.1175/JPO-D-17-0225.1.

Klymak, J.M., Balwada, D., Garabato, A.N., Abernathey, R., 2021. Parameterizing non-propagating form drag over rough bathymetry. Journal of Physical Oceanography 51. doi:10.1175/JPO-D-20-0112.1.

Kunze, E., Lien, R.C., 2019. Energy Sinks for Lee Waves in Shear Flow. Journal of Physical Oceanography 49, 2851–2865. doi:10.1175/JPO-D-19-0052.1.

Kurtakoti, P., Veneziani, M., Stössel, A., Weijer, W., 2018. Preconditioning and formation of Maud Rise polynyas in a high-resolution earth system model. Journal of Climate 31, 9659–9678. doi:10.1175/JCLI-D-18-0392.1.

LaCasce, J.H., Ferrari, R., Marshall, J., Tulloch, R., Balwada, D., Speer, K., 2014. Float-Derived Isopycnal Diffusivities in the DIMES Experiment. Journal of Physical Oceanography 44, 764–780. doi:10.1175/JPO-D-13-0175.1.

Large, W.G., McWilliams, J.C., Doney, S., 1994. Oceanic vertical mixing: A review and a model with a nonlocal boundary layer parameterization. Rev. Geophys. 32, 363–403. doi:10.1029/94RG01872.

de Lavergne, C., Madec, G., Le Sommer, J., Nurser, A.J.G., Naveira Garabato, A.C., 2016. On the consumption of Antarctic Bottom Water in the abyssal ocean. Journal of Physical Oceanography 46, 635–661. doi:10.1175/JPO-D-14-0201.1.

de Lavergne, C., Madec, G., Roquet, F., Holmes, R., McDougall, T.J., 2017. Abyssal ocean overturning shaped by seafloor distribution. Nature 551, 181–186.

Ledwell, J.R., St. Laurent, L.C., Girton, J.B., Toole, J.M., 2011. Diapycnal mixing in the Antarctic Circumpolar Current. J. Phys. Oceanogr. 41, 241–246. doi:10.1175/2010JPO4557.1.

Lin, X., Zhai, X., Wang, Z., Munday, D.R., 2018. Mean, Variability, and Trend of Southern Ocean Wind Stress: Role of Wind Fluctuations. Journal of Climate 31, 3557–3573. doi:10.1175/JCLI-D-17-0481.1.

Llort, J., Langlais, C., Matear, R., Moreau, S., Lenton, A., Strutton, P.G., 2018. Evaluating southern ocean carbon eddy-pump from biogeochemical-argo floats. Journal of Geophysical Research: Oceans 123, 971–984. doi:10.1002/2017JC012861.

Lu, J., Speer, K., 2010. Topography, jets and eddy mixing in the Southern Ocean. J. Mar. Res. 68, 479–502.

MacCready, P., Rhines, P.B., 2001. Meridional transport acros a zonal channel: Topographic

localization. J. Phys. Oceanogr. 31, 1427–1439.

Manucharyan, G.E., Spall, M.A., 2016. Wind-driven freshwater buildup and release in the Beaufort Gyre constrained by mesoscale eddies. Geophy. Res. Lett. 43, 273–282.

Marshall, D., 1997. Subduction of water masses in an eddying ocean. J. Mar. Res. 55, 201–222.

Marshall, D.P., Ambaum, M.H.P., Maddison, J.R., Munday, D.R., Novak, L., 2017. Eddy saturation and friction control of the Antarctic Circumpolar Current. Geophys. Res. Lett. 44, 286–292.

Marshall, J., Radko, T., 2003. Residual-mean solutions for the Antarctic Circumpolar Current and its associated overturning circulation. J. Phys. Oceanogr. 33, 2341–2354.

Marshall, J., Shuckburgh, E., Jones, H., Hill, C., 2006. Estimates and implications of surface eddy diffusivity in the Southern Ocean derived from tracer transport. J. Phys. Oceanogr. 36, 1806–1821.

Marshall, J., Speer, K., 2012. Closure of the meridional overturning circulation through Southern Ocean upwelling. Nature Geoscience 5, 171–180. doi:10.1038/ngeo1391.

Martinson, D.G., Iannuzzi, R.A., 1998. Antarctic ocean-ice interaction: Implications from ocean bulk property distributions in the Weddell Gyre, in: Jeffries, M.O. (Ed.), Antarctic Sea Ice: Physical Processes, Interactions and Variability. Amer. Geophys. Union. volume 74, pp. 243–271. doi:10.1029/AR074p0243.

Martinson, D.G., McKee, D.C., 2012. Transport of warm Upper Circumpolar Deep Water onto the western Antarctic Peninsula continental shelf. Ocean Sci. 8, 433–442.

Mashayek, A., Ferrari, R., Merrifield, S., Ledwell, J.R., , Laurent, L.S., Garabato, A.N., 2017a. Topographic enhancement of vertical turbulent mixing in the Southern Ocean. Nature Communications 8. doi:10.1038/ncomms14197.

Mashayek, A., Ferrari, R., Nikurashin, M., Peltier, W.R., 2015. Influence of Enhanced Abyssal Diapycnal Mixing on Stratification and the Ocean Overturning Circulation. Journal of Physical Oceanography 45, 2580–2597. doi:10.1175/JPO-D-15-0039.1.

Mashayek, A., Salehipour, H., Bouffard, D., Caulfield, C.P., Ferrari, R., Nikurashin, M., Peltier, W.R., Smyth, W.D., 2017b. Efficiency of turbulent mixing in the abyssal ocean circulation. Geophysical Research Letters 44, 6296–6306. doi:10.1002/2016GL072452.

Mazloff, M.R., Ferrari, R., Schneider, T., 2013. The force balance of the Southern Ocean overturning circulation. J. Phys. Oceanogr. 43.

McDougall, T.J., Ferrari, R., 2017. Abyssal upwelling and downwelling driven by near-boundary mixing. Journal of Physical Oceanography 47, 261–283. doi:10.1175/JPO-D-16-0082.1.

McWilliams, J.C., 2016. Submesoscale currents in the ocean. Proceedings of the Royal Society A: Mathematical, Physical and Engineering Sciences 472, 20160117. doi:10.1098/rspa.2016.0117.

Meijers, A.J., Bindoff, N.L., Roberts, J.L., 2007. On the total, mean, and eddy heat and freshwater transports in the Southern Hemisphere of a 1/8°× 1/8° global ocean model. Journal of Physical Oceanography 37, 277–295. doi:10.1175/JPO3012.1.

Melet, A., Hallberg, R., Legg, S., Nikurashin, M., 2014. Sensitivity of the ocean state to lee wave–driven mixing. Journal of Physical Oceanography 44, 900–921. doi:10.1175/JPO-D-13-072.1.

Meneghello, G., Marshall, J., Cole, S.T., Timmermans, M.L., 2017. Observational inferences of lateral eddy diffusivity in the halocline of the Beaufort Gyre. Geophys. Res. Lett. 44, 12331–12338.

Meredith, M.P., Hogg, A.M., 2006. Circumpolar response of Southern Ocean eddy activity to a change in the Southern Annular Mode. Geophys. Res. Lett. 33. L16608, doi:10.1029/2006GL026499.

Meredith, M.P., Naveira Garabato, A.C., Gordon, A.L., Johnson, G.C., 2008. Evolution of the deep and bottom waters of the Scotia Sea, Southern Ocean, during 1995–2005. J. Climate 21,

3327–3343.

Meredith, M.P., Schofield, O., Newman, L., Urban, E., Sparrow, M., 2013. The vision for a Southern Ocean Observing System. Curr. Op. Env. Sus. 5, 306–313.

Meyer, A., Polzin, K.L., Sloyan, B.M., Phillips, H.E., 2016. Internal waves and mixing near the Kerguelen Plateau. Journal of Physical Oceanography 46, 417–437. doi:10.1175/JPO-D-15-0055.1.

Meyer, A., Sloyan, B.M., Polzin, K.L., Phillips, H.E., Bindoff, N.L., 2015. Mixing variability in the Southern Ocean. Journal of Physical Oceanography 45, 966–987. doi:10.1175/JPO-D-14-0110.1.

Morrison, A.K., Griffies, S.M., Winton, M., Anderson, W.G., Sarmiento, J.L., 2016. Mechanisms of Southern Ocean heat uptake and transport in a global eddying climate model. Journal of Climate 29, 2059 – 2075. doi:10.1175/JCLI-D-15-0579.1.

Naveira Garabato, A.C., Ferrari, R., Polzin, K.L., 2011. Eddy stirring in the Southern Ocean. J. Geophys. Res. 116, C09019.

Naveira Garabato, A.C., Frajka-williams, E.E., Spingys, C.P., Legg, S., Polzin, K.L., Forryan, A., Abrahamsen, E.P., Buckingham, C.E., Griffies, S.M., Mcphail, S.D., Nicholls, K.W., Thomas, L., Meredith, M.P., 2019. Rapid mixing and exchange of deep-ocean waters in an abyssal boundary current. Proceedings of the National Academy of Sciences 116(27), 13233–13238. doi:10.1073/pnas.1904087116.

Naveira Garabato, A.C., Jullion, L., Stevens, D.P., Heywood, K.J., King, B.A., 2009. Variability of Subantarctic Mode Water and Antarctic Intermediate Water in the Drake Passage during the Late-Twentieth and Early-Twenty-First Centuries. Journal of Climate 22, 3661–3688. doi:10.1175/2009JCLI2621.1.

Naveira Garabato, A.C., Polzin, K.L., Ferrari, R., Zika, J.D., Forryan, A., 2016. A microscale view of mixing and overturning across the Antarctic Circumpolar Current. J. Phys. Oceanogr. 46, 233–254.

Naveira Garabato, A.C., Polzin, K.L., King, B.A., Heywood, K.J., Visbeck, M., 2004. Widespread intense turbulent mixing in the Southern Ocean. Science 303, 210–213.

Naveira Garabato, A.C., Stevens, D.P., Watson, A.J., Roether, W., 2007. Short-circuiting of the overturning circulation in the Antarctic Circumpolar Current. Nature 447, 194–197. doi:10.1038/nature05832.

Nicholson, S.A., Lévy, M., Jouanno, J., Capet, X., Swart, S., Monteiro, P.M.S., 2019. Iron supply pathways between the surface and subsurface waters of the Southern Ocean: From winter entrainment to summer storms. Geophysical Research Letters 46, 14567–14575. doi:10.1029/2019GL084657.

Nicholson, S.A., Lévy, M., Llort, J., Swart, S., Monteiro, P.M.S., 2016. Investigation into the impact of storms on sustaining summer primary productivity in the Sub-Antarctic ocean. Geophysical Research Letters 43, 9192–9199. doi:10.1002/2016GL069973.

Nikurashin, M., Ferrari, R., 2010a. Radiation and dissipation of internal waves generated by geostrophic motions impinging on small-scale topography: Application to the Southern Ocean. Journal of Physical Oceanography 40, 2025–2042. doi:10.1175/2010JPO4315.1.

Nikurashin, M., Ferrari, R., 2010b. Radiation and dissipation of internal waves generated by geostrophic motions impinging on small-scale topography: Theory. Journal of Physical Oceanography 40, 1055–1074. doi:10.1175/2009JPO4199.1.

Nikurashin, M., Ferrari, R., 2011. Global energy conversion rate from geostrophic flows into internal lee waves in the deep ocean. Geophysical Research Letters 38. doi:10.1029/2011GL046576.

Nikurashin, M., Vallis, G., 2011. A theory of deep stratification and overturning circulation in the ocean. J. Phys. Oceanogr. 41, 485–502.

Nøst, O.A., Biuw, M., Tverberg, V., Lydersen, C., Hattermann, T., Zhou, Q., Smedsrud, L.H.,

Kovacs, K.M., 2011. Eddy overturning of the Antarctic Slope Front controls glacial melting in the Eastern Weddell Sea. J. Geophys. Res 116, C11014.

Nycander, J., Hieronymus, M., Roquet, F., 2015. The nonlinear equation of state of sea water and the global water mass distribution. Geophysical Research Letters 42, 7714–7721. doi:10.1002/2015GL065525.

Ogle, S.E., Tamsitt, V., Josey, S.A., Gille, S.T., Cerovečki, I., Talley, L.D., Weller, R.A., 2018. Episodic Southern Ocean heat loss and its mixed layer impacts revealed by the farthest south multiyear surface flux mooring. Geophysical Research Letters 45, 5002–5010. doi:10.1029/2017GL076909.

Oka, A., Niwa, Y., 2013. Pacific deep circulation and ventilation controlled by tidal mixing away from the sea bottom. Nature Communications 4, 2419. doi:10.1038/ncomms3419.

Olbers, D., Borowski, D., Volker, C., Wolff, J.O., 2004. The dynamical balance, transport, and circulation of the Antarctic Circumpolar Current. Antarctic Science 16, 439–470.

Orsi, A.H., Johnson, G.C., Bullister, J.L., 1999. Circulation, mixing, and production of Antarctic Bottom Water. Prog. Oceanogr. 43, 55–109.

Orsi, A.H., Smethie, W.M., Bullister, J.L., 2002. On the total input of Antarctic waters to the deep ocean: A preliminary estimate from chlorofluorocarbon measurements. Journal of Geophysical Research: Oceans 107. doi:10.1029/2001JC000976.

Orsi, A.H., Whitworth, T., Nowlin, W.D., 1995. On the meridional extent and fronts of the Antarctic Circumpolar Current. Deep-Sea Res. Pt. I 42, 641–673.

Padman, L., Siegfried, M.R., Fricker, H.A., 2018. Ocean tide influences on the Antarctic and Greenland ice sheets. Reviews of Geophysics 56, 142–184. doi:10.1002/2016RG000546.

Palóczy, A., Gille, S.T., McClean, J.L., 2018. Oceanic heat delivery to the Antarctic continental shelf: Large-scale, low-frequency variability. J. Geophys. Res. 123, 7678–7701.

Patmore, R.D., Holland, P.R., Munday, D.R., Naveira Garabato, A.C., Stevens, D.P., Meredith, M.P., 2019. Topographic control of Southern Ocean gyres and the Antarctic Circumpolar Current: A barotropic perspective. J. Phys. Oceanogr. 49, 3221–3244.

Pellichero, V., Boutin, J., Claustre, H., Merlivat, L., Sallée, J.B., Blain, S., 2020. Relaxation of wind stress drives the abrupt onset of biological carbon uptake in the Kerguelen bloom: A multisensor approach. Geophysical Research Letters 47, e2019GL085992. doi:10.1029/2019GL085992.

Pellichero, V., Sallée, J.B., Chapman, C.C., Downes, S.M., 2018. The Southern Ocean meridional overturning in the sea-ice sector is driven by freshwater fluxes. Nature Communications 9, 1789. doi:10.1038/s41467-018-04101-2.

Pellichero, V., Sallée, J.B., Schmidtko, S., Roquet, F., Charrassin, J.B., 2017. The ocean mixed layer under Southern Ocean sea-ice: Seasonal cycle and forcing. Journal of Geophysical Research: Oceans 122, 1608–1633. doi:10.1002/2016JC011970.

Pierrehumbert, R.T., 1984. Local and global baroclinic instability of zonally varying flow. J. Atmos. Sci. 41, 2141–2162.

du Plessis, M., Swart, S., Ansorge, I.J., Mahadevan, A., 2017. Submesoscale processes promote seasonal restratification in the Subantarctic Ocean. Journal of Geophysical Research: Oceans 122, 2960–2975. doi:10.1002/2016JC012494.

du Plessis, M., Swart, S., Ansorge, I.J., Mahadevan, A., Thompson, A.F., 2019. Southern Ocean Seasonal Restratification Delayed by Submesoscale Wind–Front Interactions. Journal of Physical Oceanography 49, 1035–1053. doi:10.1175/JPO-D-18-0136.1.

Pollard, R., Tréguer, P., Read, J., 2006. Quantifying nutrient supply to the southern ocean. Journal of Geophysical Research: Oceans 111. doi:10.1029/2005JC003076.

Polzin, K.L., Toole, J.M., , Schmitt, R.W., 1995. Finescale parameterizations of turbulent dissipation. J. Phys. Oceanogr. 25, 306–328.

Polzin, K.L., Toole, J.M., Ledwell, J.R., Schmitt, R.W., 1997. Spatial variability of turbulent mixing in the abyssal ocean. Science 276, 93–96.

Price, J.F., Mooers, C.N.K., Van Leer, J.C., 1978. Observation and simulation of storm-induced mixed-layer deepening. Journal of Physical Oceanography 8, 582–599. doi:10.1175/1520-0485(1978)008<0582:OASOSI>2.0.CO;2.

Redi, M.H., 1982. Oceanic isopycnal mixing by coordinate rotation. J. Phys. Oceanogr. 12, 1154–1158.

Rintoul, S.R., England, M.H., 2002. Ekman transport dominates local air–sea fluxes in driving variability of subantarctic mode water. Journal of Physical Oceanography 32, 1308–1321. doi:10.1175/1520-0485.

Roach, C.J., Balwada, D., Speer, K., 2016. Horizontal mixing in the Southern Ocean from Argo float trajectories. J. Geophys. Res. 121, 5570–5586.

Roach, C.J., Speer, K., 2019. Exchange of water between the Ross Gyre and ACC assessed by Lagrangian particle tracking. J. Geophys. Res. Oceans 124, 4631–4643.

Roemmich, D., Church, J., Gilson, J., Monselesan, D., Sutton, P., Wijffels, S., 2015. Unabated planetary warming and its ocean structure since 2006. Nature Climate Change 5, 240–245. doi:10.1038/nclimate2513.

Rosso, I., Hogg, A.M., Kiss, A.E., Gayen, B., 2015. Topographic influence on submesoscale dynamics in the Southern Ocean. Geophys. Res. Lett. 42, 1139–1147.

Rosso, I., Hogg, A.M., Strutton, P.G., Kiss, A.E., Matear, R., Klocker, A., van Sebille, E., 2014. Vertical transport in the ocean due to sub-mesoscale structures: Impacts in the Kerguelen region. Ocean Modelling 80, 10 – 23. doi:10.1016/j.ocemod.2014.05.001.

Ruan, X., Thompson, A.F., Flexas, M.M., Sprintall, J., 2017. Contribution of topographically generated submesoscale turbulence to Southern Ocean overturning. Nature Geoscience 10, 840–845. doi:10.1038/ngeo3053.

Sabine, C.L., Feely, R.A., Gruber, N., Key, R.M., Lee, K., Bullister, J.L., Wanninkhof, R., Wong, C., Wallace, D.W.R., Tilbrook, B., et al., 2004. The oceanic sink for anthropogenic $CO_2$. Science 305, 367–371. doi:10.1126/science.1097403.

Saenko, O.A., Zhai, X., Merryfield, W.J., Lee, W.G., 2012. The combined effect of tidally and eddy-driven diapycnal mixing on the large-scale ocean circulation. Journal of Physical Oceanography 42, 526–538. doi:10.1175/JPO-D-11-0122.1.

Sallée, J.B., Shuckburgh, E., Bruneau, N., Meijers, A.J.S., Bracegirdle, T.J., Wang, Z., Roy, T., 2013. Assessment of Southern Ocean water mass circulation and characteristics in CMIP5 models: Historical bias and forcing response. Journal of Geophysical Research: Oceans 118, 1830–1844. doi:10.1002/jgrc.20135.

Sallée, J.b., Speer, K., Rintoul, S., 2010. Zonally asymmetric response of the Southern Ocean mixed-layer depth to the Southern Annular Mode. Nat. Geosci. 3, 273–279. doi:10.1038/ngeo812.

Scott, R.B., Goff, J.A., Naveira Garabato, A.C., Nurser, A.J.G., 2011. Global rate and spectral characteristics of internal gravity wave generation by geostrophic flow over topography. Journal of Geophysical Research: Oceans 116. doi:10.1029/2011JC007005.

Sheen, K.L., Brearley, J.A., Naveira Garabato, A.C., Smeed, D.A., Laurent, L.S., Meredith, M.P., Thurnherr, A.M., Waterman, S.N., 2015. Modification of turbulent dissipation rates by a deep Southern Ocean eddy. Geophysical Research Letters 42, 3450–3457. doi:10.1002/2015GL063216.

Sheen, K.L., Brearley, J.A., Naveira Garabato, A.C., Smeed, D.A., Waterman, S., Ledwell, J.R., Meredith, M.P., St. Laurent, L., Thurnherr, A.M., Toole, J.M., Watson, A.J., 2013. Rates and mechanisms of turbulent dissipation and mixing in the Southern Ocean: Results from the Diapycnal and Isopycnal Mixing Experiment in the Southern Ocean (DIMES). Journal of

Geophysical Research: Oceans 118, 2774–2792. doi:10.1002/jgrc.20217.

Sheen, K.L., Naveira Garabato, A.C., Brearley, J.A., Meredith, M.P., Polzin, K.L., Smeed, D.A., Forryan, A., King, B.A., Sallée, J.B., St. Laurent, L., Thurnherr, A.M., Toole, J.M., Waterman, S.N., Watson, A.J., 2014. Eddy-induced variability in southern ocean abyssal mixing on climatic timescales. Nature Geoscience 7, 577–582. doi:10.1038/ngeo2200.

Silvano, A., Rintoul, S.R., Peña Molino, B., Hobbs, W.R., van Wijk, E., Aoki, S., Tamura, T., Williams, G.D., 2018. Freshening by glacial meltwater enhances melting of ice shelves and reduces formation of Antarctic Bottom Water. Science Advances 4. doi:10.1126/sciadv.aap9467.

Silvester, J.M., Lenn, Y.D., Polton, J.A., Rippeth, T.P., Maqueda, M.M., 2014. Observations of a diapycnal shortcut to adiabatic upwelling of Antarctic Circumpolar Deep Water. Geophysical Research Letters 41, 7950–7956. doi:10.1002/2014GL061538.

Simmons, H.L., Jayne, S.R., Laurent, L.C.S., Weaver, A.J., 2004. Tidally driven mixing in a numerical model of the ocean general circulation. Ocean Modelling 6, 245 – 263. doi:10.1016/S1463-5003(03)00011-8.

Sloyan, B., 2005. Spatial variability of mixing in the Southern Ocean. Geophys. Res. Lett. 32, L18603. doi:10.1029/2005GL023568.

Sloyan, B.M., Talley, L.D., Chereskin, T.K., Fine, R., Holte, J., 2010. Antarctic Intermediate Water and Subantarctic Mode Water formation in the southeast Pacific: The role of turbulent mixing. Journal of Physical Oceanography 40, 1558 – 1574. doi:10.1175/2010JPO4114.1.

Smith, K.S., 2007. The geography of linear baroclinic instability in Earth's oceans. J. Mar. Res. 65, 655–683.

Smith, K.S., Marshall, J., 2009. Evidence for enhanced eddy mixing at middepth in the Southern Ocean. Journal of Physical Oceanography 39, 50–69. doi:10.1175/2008JPO3880.1.

Sokolov, S., Rintoul, S.R., 2009. Circumpolar structure and distribution of the Antarctic Circumpolar Current fronts: 1. Mean circumpolar paths. J. Geophys. Res. 114. C11018, doi:10.1029/2008JC005108.

Speer, K., Rintoul, S.R., Sloyan, B., 2000. The diabatic Deacon cell. J. Phys. Oceanogr. 30, 3212–3222.

Speer, K., Sallée, J.B., Pellichero, V., 2018. Antarctic Mode Water. J. Mar. Res. 76, 119–137.

St. Laurent, L., Naveira Garabato, A.C., Ledwell, J.R., Thurnherr, A.M., Toole, J.M., Watson, A.J., 2013. Turbulence and diapycnal mixing in Drake Passage. Journal of Physical Oceanography 42, 2143–2152. doi:10.1175/JPO-D-12-027.1.

St. Laurent, L.C., Toole, J.M., Schmitt, R.W., 2001. Buoyancy forcing by turbulence above rough topography in the abyssal Brazil Basin. Journal of Physical Oceanography 31, 3476–3495. doi:10.1175/1520-0485(2001)031<3476:BFBTAR>2.0.CO;2.

St-Laurent, P., Klinck, J.M., Dinniman, M.S., 2013. On the role of coastal troughs in the circulation of warm circumpolar deep water on Antarctic shelves. J. Phys. Oceanogr. 43, 51–64.

Stammer, D., 1998. On eddy characteristics, eddy transports, and mean flow properties. J. Phys. Oceanogr. 28, 727–739.

Stewart, A.L., Hogg, A.M., 2017. Reshaping the Antarctic Circumpolar Current via Antarctic Bottom Water export. J. Phys. Oceanogr. 47, 2577–2601. doi:10.1175/JPO-D-17-0007.1.

Stewart, A.L., Klocker, A., Menemenlis, D., 2018. Circum-Antarctic shoreward heat transport derived from an eddy- and tide-resolving simulation. Geophysical Research Letters 45, 834–845. doi:10.1002/2017GL075677.

Stewart, A.L., Thompson, A.F., 2013. Connecting Antarctic cross-slope exchange with Southern Ocean overturning. J. Phys. Oceanogr. 43, 1453–1471.

Stewart, A.L., Thompson, A.F., 2015. Eddy-mediated transport of warm Circumpolar Deep Water across the Antarctic Shelf Break. Geophys. Res. Lett. 42, 432–440.

von Storch, J.S., Sasaki, H., Marotzke, J., 2007. Wind-generated power input to the deep ocean: An estimate using a 1/10° general circulation model. Journal of Physical Oceanography 37, 657–672. doi:10.1175/JPO3001.1.

Su, Z., Stewart, A.L., Thompson, A.F., 2014. An idealized model of weddell gyre export variability. J. Phys. Oceanogr. 44, 1671–1688.

Su, Z., Wang, J., Klein, P., Thompson, A.F., Menemenlis, D., 2018. Ocean submesoscales as a key component of the global heat budget. Nat. Commun. 9, 775. doi:10.1038/s41467-018-02983-w.

Sun, S., Eisenman, I., Stewart, A.L., 2018. Does Southern Ocean surface forcing shape the global ocean overturning circulation? Geophys. Res. Lett. 45, 2413–2423.

Swart, N.C., Gille, S.T., Fyfe, J.C., Gillett, N.P., 2018a. Recent Southern Ocean warming and freshening driven by greenhouse gas emissions and ozone depletion. Nature Geoscience 11, 836–841. doi:10.1038/s41561-018-0226-1.

Swart, S., Campbell, E.C., Heuzé, C.H., Johnson, K., Lieser, J.L., Massom, R., Mazloff, M., Meredith, M., Reid, P., Sallée, J.B., Stammerjohn, S., 2018b. Return of the Maud Rise polynya: Climate litmus or sea ice anomaly? [in "State of the Climate in 2017. Bull. Amer. Meteor. Soc. 99, S188–S198. doi:10.1175 /2018BAMSStateoftheClimate.1.

Swart, S., du Plessis, M.D., Thompson, A.F., Biddle, L.C., Giddy, I., Linders, T., Mohrmann, M., Nicholson, S.A., 2020. Submesoscale fronts in the Antarctic marginal ice zone and their response to wind forcing. Geophysical Research Letters 47, e2019GL086649. doi:10.1029/2019GL086649.

Swart, S., Thomalla, S.J., Monteiro, P.M.S., 2015. The seasonal cycle of mixed layer dynamics and phytoplankton biomass in the Sub-Antarctic Zone: A high-resolution glider experiment. Journal of Marine Systems 147, 103 – 115. doi:10.1016/j.jmarsys.2014.06.002.

Takahashi, A., Hibiya, T., 2019. Assessment of finescale parameterizations of deep ocean mixing in the presence of geostrophic current shear: Results of microstructure measurements in the Antarctic Circumpolar Current region. Journal of Geophysical Research: Oceans 124, 135–153. doi:10.1029/2018JC014030.

Talley, L.D., 2013. Closure of the global overturning circulation through the Indian, Pacific, and Southern Oceans: Schematics and transports. Oceanography 26, 80–97. doi:10.5670/oceanog.2013.07.

Tamsitt, V., Cerovečki, I., Josey, S.A., Gille, S.T., Schulz, E., 2020. Mooring observations of air–sea heat fluxes in two Subantarctic Mode Water formation regions. Journal of Climate 33, 2757–2777. doi:10.1175/JCLI-D-19-0653.1.

Tamsitt, V., Drake, H., Morrison, A.K., Talley, L.D., Dufour, C.O., Gray, A.R., Griffies, S.M., Mazloff, M.R., Sarmiento, J.L., Wang, J., Weijer, W., 2017. Spiraling up: pathways of global deep waters to the surface of the southern ocean. Nat. Comm. , in press.

Taylor, J.R., Bachman, S., Stamper, M., Hosegood, P., Adams, K., Sallee, J.B., Torres, R., 2018. Submesoscale Rossby waves on the Antarctic Circumpolar Current. Science Advances 4. doi:10.1126/sciadv.aao2824.

Thomas, L.N., 2005. Destruction of potential vorticity by winds. Journal of Physical Oceanography 35, 2457–2466. doi:10.1175/JPO2830.1.

Thomas, L.N., Tandon, A., Mahadevan, A., 2008. Submesoscale processes and dynamics, in: Hecht, M.W., Hasumi, H. (Eds.), Ocean Modeling in an Eddying Regime. American Geophysical Union (AGU), pp. 17–38. doi:10.1029/177GM04.

Thompson, A.F., Haynes, P.H., Wilson, C., Richards, K.J., 2010. Rapid Southern Ocean front transitions in an eddy-resolving ocean GCM. Geophys. Res. Lett. 37, L23602.

Thompson, A.F., Heywood, K.J., Schmidtko, S., Stewart, A.L., 2014. Eddy transport as a key component of the antarctic overturning circulation. Nature Geosci 7, 879–884.

Thompson, A.F., Naveira Garabato, A.C., 2014. Equilibration of the Antarctic Circumpolar Current by standing meanders. J. Phys. Oceanogr. 44, 1811–1828.

Thompson, A.F., Sallée, J.B., 2012. Jets and topography: Jet transitions and the impact on transport in the Antarctic Circumpolar Current. J. Phys. Oceanogr. 42, 956–972.

Thompson, A.F., Stewart, A.L., Spence, P., Heywood, K.J., 2018. The Antarctic Slope Current in a changing climate. Rev. Geophys. 56, 741–770.

Thorpe, S.A., 2005. The Turbulent Ocean. Cambridge University Press, Cambridge. doi:10.1017/CBO9780511819933.

Toggweiler, J.R., Samuels, B., 1998. On the ocean's large-scale circulation near the limit of no vertical mixing. J. Phys. Oceanogr 28, 1832–1852. doi:152, 10.1175/1520-0485(1998)028<1832:OTOSLS>2.0.CO;2.

Treguier, A.M., McWilliams, J.C., 1990. Topographic influences on wind-driven, stratified flow in a $\beta$-plane channel: An idealized model for the Antarctic Circumpolar Current. Journal of Physical Oceanography 20, 321–343. doi:10.1175/1520-0485(1990)020<0321:TIOWDS>2.0.CO;2.

Trossman, D.S., Arbic, B.K., Richman, J., Garner, S.T., Jayne, S., Wallcraft, A., 2016. Impact of topographic internal lee-wave drag on an eddying global ocean model. Ocean Modell. 97, 109–128. doi:10.1016/j.ocemod.2015.10.013.

Tulloch, R., Ferrari, R., Jahn, O., Klocker, A., LaCasce, J., Ledwell, J.R., Marshall, J., Messias, M.J., Speer, K., Watson, A., 2014. Direct estimate of lateral eddy diffusivity upstream of Drake Passage. Journal of Physical Oceanography 44, 2593–2616. doi:10.1175/JPO-D-13-0120.1.

Uchida, T., Balwada, D., Abernathey, R., McKinley, G., Smith, S., Lévy, M., 2019. The contribution of submesoscale over mesoscale eddy iron transport in the open Southern Ocean. Journal of Advances in Modeling Earth Systems 11, 3934–3958. doi:10.1029/2019MS001805.

Uchida, T., Balwada, D., P. Abernathey, R., A. McKinley, G., K. Smith, S., Lévy, M., 2020. Vertical eddy iron fluxes support primary production in the open Southern Ocean. Nature Communications 11, 1125. doi:10.1038/s41467-020-14955-0.

Vernet, M., Geibert, W., Hoppema, M., Brown, P.J., Haas, C., adn W. Jokat, H.H.H., Jullion, L., Mazloff, M., Bakker, D.C.E., Brearley, J.A., Croot, P., Hattermann, T., Hauck, J., Hillenbrand, C.D., Hoppe, C.J.M., Huhn, O., Koch, B.P., Lechtenfeld, O.J., Meredith, M.P., Garabato, A.C.N., Nöthig, E.M., Peeken, I., van der Loeff, M.M.R., Schmidtko, S., Schröder, M., Strass, V.H., Torres-Valdés, S., Verdy, A., 2019. The Weddell Gyre, Southern Ocean: Present knowledge and future challenges. Ann. Rev. Fluid Mech. 57, 623–708.

Viglione, G.A., Thompson, A.F., Flexas, M.M., Sprintall, J., Swart, S., 2018. Abrupt transitions in submesoscale structure in southern Drake Passage: Glider observations and model results. Journal of Physical Oceanography 48, 2011–2027. doi:10.1175/JPO-D-17-0192.1.

Volkov, D.L., Fu, L.L., Lee, T., 2010. Mechanisms of the meridional heat transport in the Southern Ocean. Ocean Dynamics 60, 791–801. doi:10.1007/s10236-010-0288-0.

Waterman, S., Naveira Garabato, A.C., Polzin, K.L., 2013. Internal waves and turbulence in the Antarctic Circumpolar Current. Journal of Physical Oceanography 43, 259–282. doi:10.1175/JPO-D-11-0194.1.

Waterman, S., Polzin, K.L., Naveira Garabato, A.C., Sheen, K.L., Forryan, A., 2014. Suppression of internal wave breaking in the Antarctic Circumpolar Current near topography. Journal of Physical Oceanography 44, 1466–1492. doi:10.1175/JPO-D-12-0154.1.

Watson, A.J., Ledwell, J.R., Messias, M.J., King., B.A., Mackay, N., Meredith, M.P., Mills, B., Naveira Garabato, A.C., 2014. Rapid cross-density ocean mixing at mid-depths in the Drake Passage measured by tracer release. Nature 501, 408–411. doi:doi:10.1038/nature12432.

Watson, A.J., Naveira Garabato, A.C., 2006. The role of Southern Ocean mixing and upwelling in glacial-interglacial atmospheric $CO_2$ change. Tellus B: Chemical and Physical Meteorology 58,

73–87. doi:10.1111/j.1600-0889.2005.00167.x.

Whitt, D.B., Lévy, M., Taylor, J.R., 2017. Low-frequency and high-frequency oscillatory winds synergistically enhance nutrient entrainment and phytoplankton at fronts. Journal of Geophysical Research: Oceans 122, 1016–1041. doi:10.1002/2016JC012400.

Whitt, D.B., Nicholson, S.A., Carranza, M.M., 2019. Global impacts of subseasonal (<60 day) wind variability on ocean surface stress, buoyancy flux, and mixed layer depth. Journal of Geophysical Research: Oceans 124, 8798–8831. doi:10.1029/2019JC015166.

Wilson, E.A., Riser, S.C., Campbell, E.C., Wong, A.P.S., 2019. Winter upper-ocean stability and ice–ocean feedbacks in the sea ice–covered Southern Ocean. Journal of Physical Oceanography 49, 1099–1117. doi:10.1175/JPO-D-18-0184.1.

Witter, D.L., Chelton, D.B., 1998. Eddy–mean flow interaction in zonal oceanic jet flow along zonal ridge topography. J. Phys. Oceanogr. 28, 2019–2039.

Wolfe, C.L., Cessi, P., 2011. The adiabatic pole-to-pole overturning circulation. J. Phys. Oceanogr. 41, 1795–1810.

Wright, C.J., Scott, R.B., Ailliot, P., Furnival, D., 2014. Lee wave generation rates in the deep ocean. Geophysical Research Letters 41, 2434–2440. doi:10.1002/2013GL059087.

Wunsch, C., 1998. The work done by the wind on the oceanic general circulation. Journal of Physical Oceanography 28, 2332–2340. doi:10.1175/1520-0485(1998)028<2332:TWDBTW>2.0.CO;2.

Yang, L., Nikurashin, M., Hogg, A.M., Sloyan, B.M., 2018. Energy loss from transient eddies due to lee wave generation in the Southern Ocean. Journal of Physical Oceanography 48, 2867–2885. doi:10.1175/JPO-D-18-0077.1.

Youngs, M.K., Thompson, A.F., Lazar, A., Richardss, K.J., 2017. ACC meanders, energy transfer, and mixed barotropic-baroclinic instability. J. Phys. Oceanogr. 47, 1291–1305.

Yuan, X., 2004. High-wind-speed evaluation in the Southern Ocean. Journal of Geophysical Research: Atmospheres 109. doi:10.1029/2003JD004179.

Zika, J.D., Sallée, J.B., Meijers, A.J.S., Naveira Garabato, A.C., Watson, A.J., Messias, M.J., King, B.A., 2020. Tracking the spread of a passive tracer through Southern Ocean water masses. Ocean Sci. 16, 323–336.

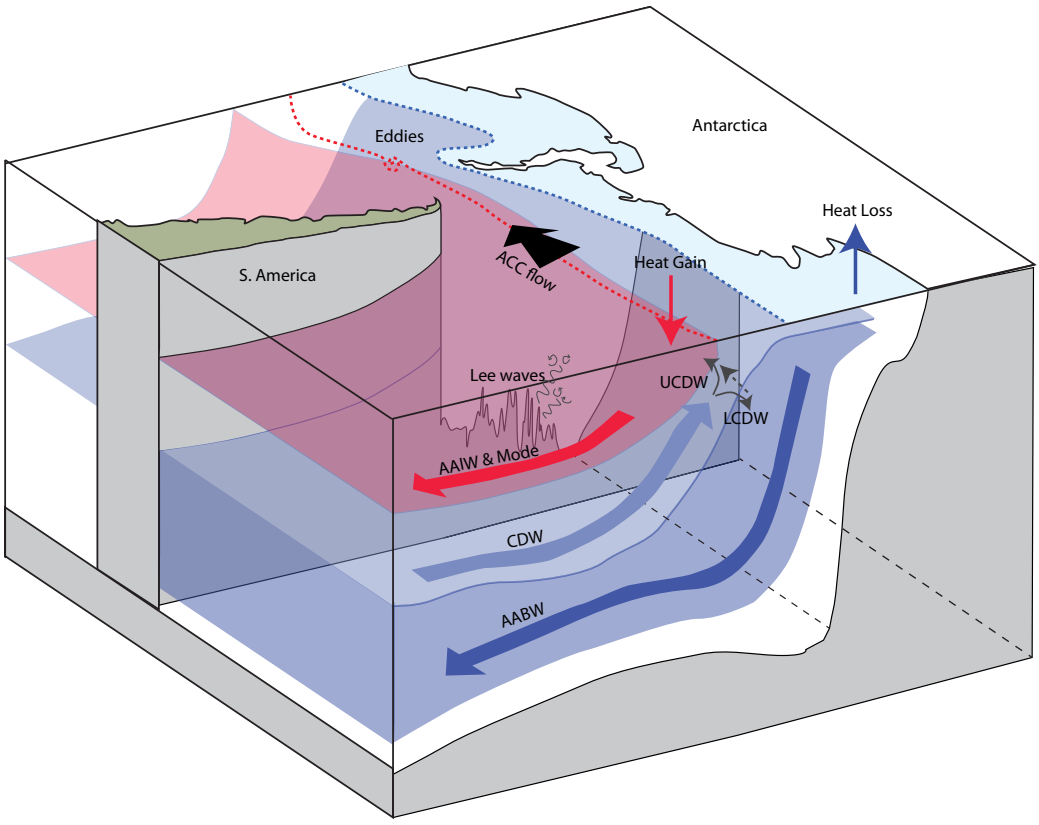


**FIGURE 12.1** Schematic large-scale circulation in the Southern Ocean, showing the Antarctic Circumpolar Current (ACC) flowing eastward (black arrow), Circumpolar Deep Water (CDW) upwelling at about the same latitude as the ACC (light blue arrow), and the upper and lower cells of the meridional overturning circulation. Upper Circumpolar Deep Water (UCDW) advects northward and contributes to Antarctic Intermediate Water and Mode water formation. Lower Circumpolar Deep Water (LCDW) loses heat near Antarctica and sinks to form Antarctic Bottom Water (AABW).

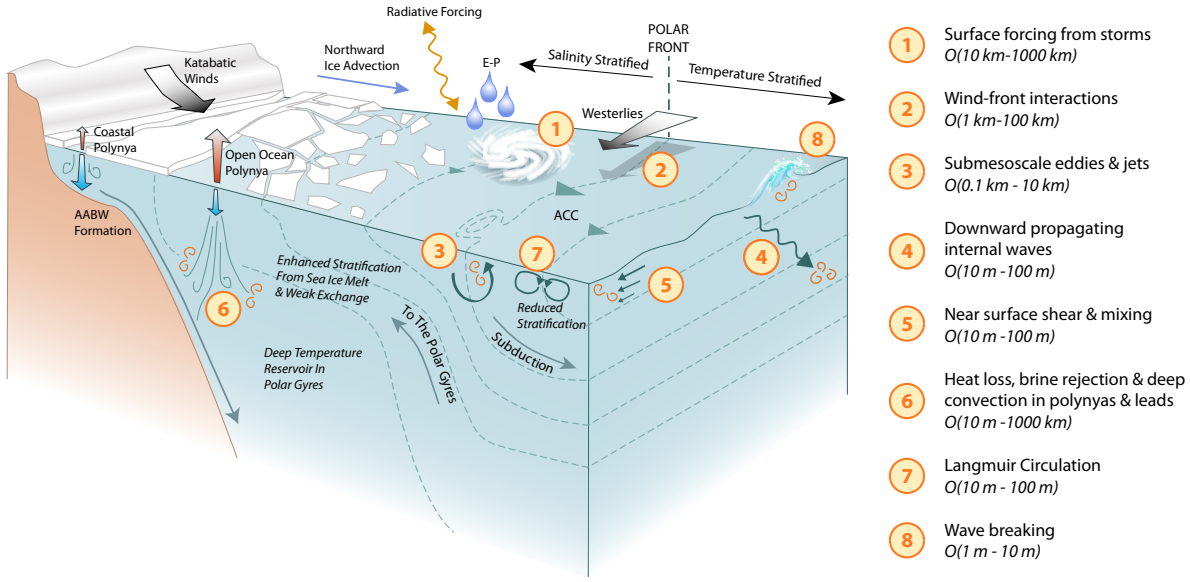


**FIGURE 12.2** Conceptual view of the main processes driving mixing in the upper cell of the Southern Ocean. It includes mixing processes spanning the open-ocean ACC domains, dominated by surface winds and waves, to the sea ice and ice shelf-impacted regions of the Southern Ocean. An estimated scale for each mixing processes is indicated.

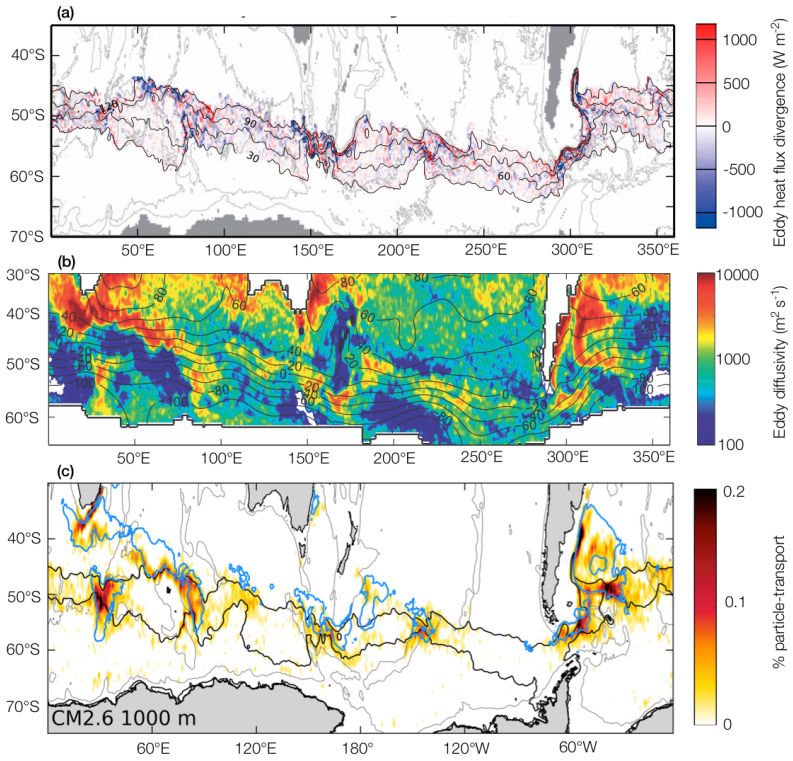


**FIGURE 12.3** Examples of the impact of flow-topography interactions on mixing properties and adiabatic transport in the Southern Ocean. (a) The vertically integrated divergence of the transient eddy heat flux (W $m^{-2}$) in the ACC region, calculated from the Southern Ocean State Estimate (SOSE). (b) Map of the eddy diffusivity [log10 ($m^2$ $s^{-1}$)] for the full Southern Ocean. This estimate is derived from satellite altimetry-derived surface velocities and, through the use of both anomaly and time-mean sea surface heights measurements, includes an estimate of mean-flow suppression. This suppression is enhanced outside of standing meander regions. (c) Upwelling of passively advected particles across the 1000 m isobar from the CM2.6 numerical simulation. Upwelling, largely linked to lateral motion along tilted isopycnals, occurs preferentially in the lee of topographic features. Figure adapted from Abernathey and Cessi (2014); Ferrari and Nikurashin (2010); Tamsitt et al. (2017).

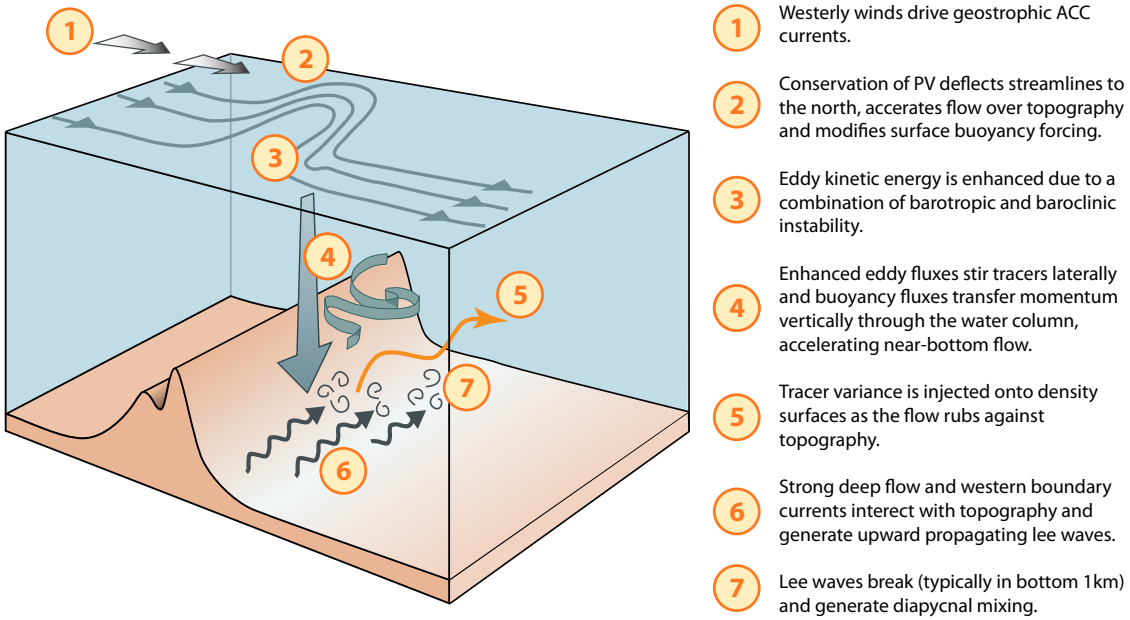


**FIGURE 12.4** Schematic showing the pathway through which wind energy is transferred through the water column and converted into turbulent mixing through lee wave generation and breaking. Arrow widths represent approximate relative power fluxes, with wind into geostrophic flow being roughly 1 TW globally. About half of all global lee wave generation occurs in the Southern Ocean. Standing meanders are regions where isopycnal and diapycnal processes are closely linked as (adiabatic) eddy buoyancy fluxes, enhanced in the lee of topography, transfer momentum to the deep ocean.

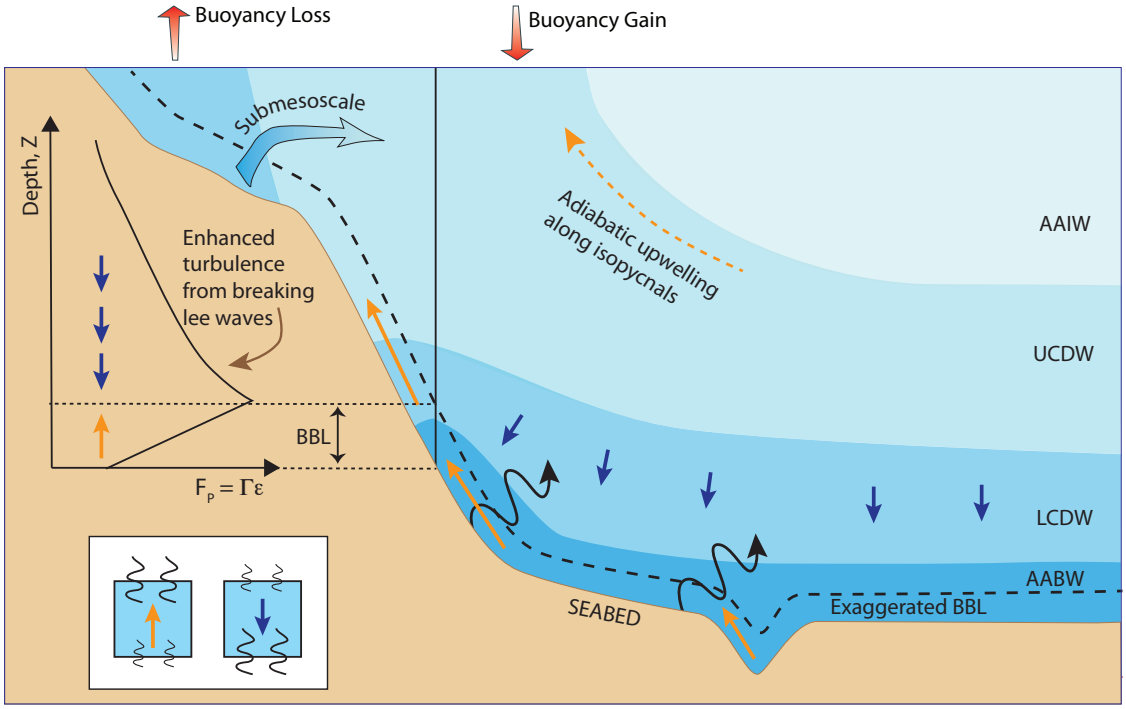


**FIGURE 12.5** A depth-longitude section of the Southern Ocean, including the bottom-boundary layer (BBL, black dashed line). The BBL is shown with an exaggerated thickness to illustrate the effect of near-boundary mixing. Lee waves (black wiggly arrows) generated at rough topography form a region of enhanced turbulence and strong density flux, typically within 1 km of the seabed, as is apparent on the vertical turbulent density flux profile sketched on the left of the figure. The weakly stratified boundary layer is characterized by reduced stratification and density flux. Solid orange arrows indicate BBL diabatic along-boundary upwelling, and solid blue arrows show the diabatic sinking of waters in the ocean interior. Blue colored bands represent water masses of Antarctic Intermediate Water (AAIW), Upper Circumpolar Deep Water (UCDW), Lower Circumpolar Deep Water (LCDW) and Antarctic Bottom Water (AABW), the boundaries of which delineate isopycnals (note they intersect the seabed at right-angles to satisfy the condition of zero buoyancy flux across the seafloor). Submesoscale flows can also catalyze near-boundary mixing, here represented by the blue/orange arrow transforming LCDW into lighter waters. Isopycnals of waters in the upper overturning cell (e.g. UCDW and AAIW) outcrop at the surface, allowing these lighter, adiabatically upwelled waters (orange dashed arrow) to undergo diabatic transformation by surface processes. The inset at bottom left illustrates how vertical variations in mixing modify a water parcel: stronger mixing on the upper face results in more buoyancy being gained from above as compared to buoyancy lost from below, a reduction of density, and upwelling of the parcel (and vice versa). Note that this schematic does not include AABW formation processes and the associated down-slope flow of bottom waters.

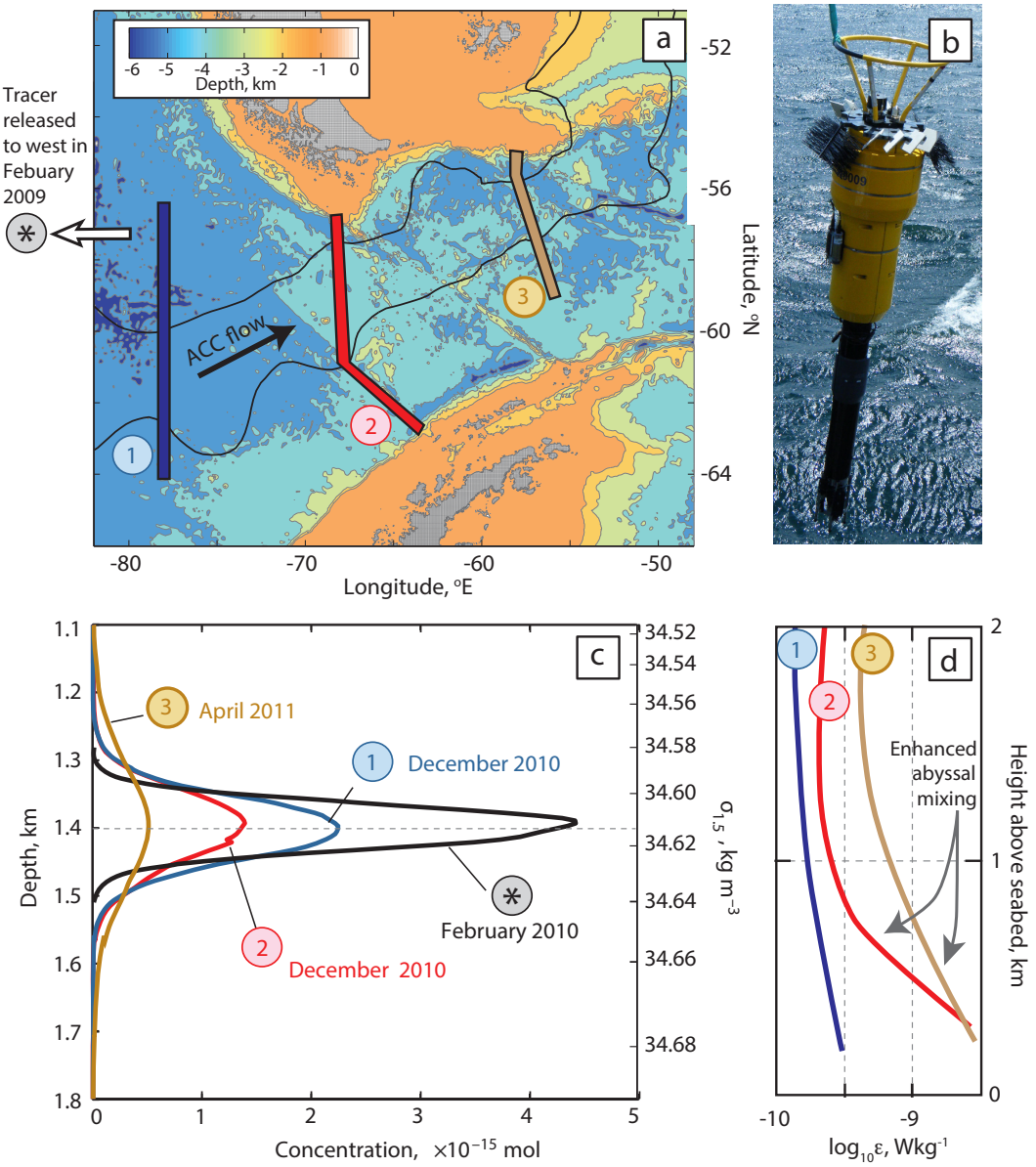


**FIGURE 12.6** The DIMES field program. (a) The DIMES study region with location of three of the tracer and microstructure measurement sections marked: 1 - Section at 78 W December 2010, 2 - Western Drake Passage section December 2010, 3 - Eastern Drake Passage section, April 2011. Background contours show bathymetry - note smooth seabed in the East Pacific and contrasting rough topography within Drake Passage. Black lines show rough positions of the sub-Antarctic Front and the Polar Front. (b) Vertical microstructure profiler (VMP) being deployed in Drake Passage. Photograph from K.Sheen. (c) Mean depth profiles of tracer concentrations obtained from the three sections shows in panel a, plus a survey conducted in the East Pacific, 1 year after tracer release (black line). Figure adapted from Watson et al. (2014). (d) Representative profiles of section averaged turbulent dissipation rates averaged as measured by the VMP, based on data presented in Sheen et al. (2013). Note the enhanced mixing within the bottom 1 km. Panels c and d demonstrate the increased diapycnal mixing within the southwest Atlantic compared to the southeast Pacific.